Hyperdiverse archaea near life limits at the polyextreme geothermal Dallol area

Jodie Belilla, David Moreira, Ludwig Jardillier, Guillaume Reboul, Karim Benzerara, José M López-García, Paola Bertolino, Ana I López-Archilla, Purificación López-García

Hyperdiverse archaea near life limits at the polyextreme geothermal Dallol area

Jodie Belilla[1], David Moreira[1], Ludwig Jardillier[1], Guillaume Reboul[1], Karim Benzerara[2], José M. López-García[3], Paola Bertolino[1], Ana I. López-Archilla[4] & Purificación López-García[1*]

[1] Ecologie Systématique Evolution, CNRS, Université Paris-Sud, AgroParisTech, Université Paris-Saclay, Orsay, France.

[2] Institut de Minéralogie, de Physique des Matériaux et de Cosmochimie, CNRS, Université Pierre et Marie Curie, Muséum National d'Histoire Naturelle, IRD, Sorbonne Universités, Paris, France.

[3] Instituto Geológico y Minero de España, Palma de Mallorca, Spain.

[4] Departamento de Ecología, Universidad Autónoma de Madrid, Madrid, Spain

*Correspondence to: puri.lopez@u-psud.fr

Microbial life has adapted to various individual extreme conditions; yet, organisms simultaneously adapted to very low pH, high salt and high temperature are unknown. We combined environmental 16S/18S rRNA-gene metabarcoding, cultural approaches, fluorescence-activated cell sorting, scanning electron microscopy and chemical analyses to study samples along such unique polyextreme gradients in the Dallol-Danakil area (Ethiopia). We identify two physicochemical barriers to life in the presence of surface liquid water defined by: i) high chaotropicity-low water activity in Mg^{2+}/Ca^{2+}-dominated brines and ii) hyperacidity-salt combinations (pH~0/ NaCl-dominated salt-saturation). When detected, life was dominated by highly diverse ultrasmall archaea widely distributed across phyla with and without previously known halophilic members. We hypothesize that high cytoplasmic K^{+}-level was an original archaeal adaptation to hyperthermophily, subsequently exapted during multiple transitions to extreme halophily. We detect active silica encrustment/fossilization of cells but also abiotic biomorphs of varied chemistry. Our work helps circumscribing habitability and calls for cautionary interpretations of morphological biosignatures on Earth and beyond.

Microbial life has adapted to so-called extreme values of temperature, pH or salinity, but also to several polyextreme, e.g. hot acidic or salty alkaline, ecosystems[1,2]. Various microbial lineages have been identified in acidic brines in the pH range 1.5-4.5, e.g. in Western Australia[3,4] and Chile[3]. However, although some acidophilic archaea thrive at pH~0 (*Picrophilus oshimae* grows at an optimal pH of 0.7)[5] and many halophilic archaea live in hypersaline systems (>30%; NaCl-saturation conditions), organisms adapted simultaneously to very low pH (<1) and high salt, and eventually also high temperature, are not known among cultured prokaryotic species[1]. Are molecular adaptations to these combinations incompatible or (hot) hyperacidic hypersaline environments simply rare and unexplored? The Dallol geothermal dome and its surroundings (Danakil Depression, Afar, Ethiopia) allow to address this question by offering unique polyextreme gradients combining high salt content (33 to >50%; either Mg^{2+}/Ca^{2+} or $Na^{+}(/Fe^{2+/3+})$-rich), high temperature (25-110°C) and low pH (≤-1.5 to 6).

Dallol is an up-lifted (~40 m) dome structure located in the North of the Danakil depression (~120 m below-sea-level), a 200 km-long basin within the Afar rift, at the triple junction between the Nubian, Somalian and Arabian Plates[6]. Lying only 30 km north of the hypersaline, hydrothermally-influenced, Lake Assale (Karum) and the Erta Ale volcanic range, Dallol does not display volcanic outcrops but intense degassing and hydrothermalism. These activities are observed on the salt dome and the adjacent Black Mountain and Yellow Lake (Gaet'Ale) areas[6,7] (Fig. 1a-b). Gas and fluid isotopic measurements indicate that meteoritic waters, notably infiltrating from the high Ethiopian plateau (>2,500 m), interact with an underlying geothermal reservoir (280-370°C)[7,8]. Further interaction of those fluids with the km-thick marine evaporites filling the Danakil depression results in unique combinations of polyextreme conditions and salt chemistries[6,7,9,10], which have led some authors consider Dallol as a Mars analog[11].

Here, we use environmental 16S/18S rRNA-gene metabarcoding, cultural approaches, fluorescence-activated cell sorting and scanning electron microscopy combined with chemical analyses to explore microbial occurrence, diversity and potential fossilization along Dallol-Danakil polyextreme gradients[12,13,14,15].

Results and Discussion

To investigate the distribution and, eventually, type of microbial life along those polyextreme gradients, we analyzed a large variety of brine and mineral samples collected mainly in two field expeditions (January 2016 and 2017; a few additional samples were collected in 2018) in four major zones (Fig. 1, Extended Data Figs. 1-2, Extended Data Table 1). The first zone corresponded to the

hypersaline (37-42%) hyperacidic (pH between ~0 and -1; values down to -1.6 were measured on highly concentrated and oxidized brines on site) and sometimes hot (up to 108°C) colorful ponds on the top of the Dallol dome (Fig. 1c, Extended Data Figs. 1a and 2a-h, Extended Data Table 1). The second zone comprised the salt canyons located at the Southwestern extremity of the Dallol dome and the Black Mountain area that includes the Black Lake (Figs. 1b and 1d; Extended Data Figs. 1b-c and 2l-q). Brine samples collected in a cave reservoir (Gt samples) and in ephemeral pools with varying degrees of geothermal influence at the dome base (PS/PS3) were hypersaline (~35%), with moderate temperature (~30°C) and acidity (pH ~4-6). By contrast, pools located near the small (~15 m diameter), extremely hypersaline (>70%), hot (~70°C) and acidic (pH~3) Black Lake were slightly more acidic (pH~3), warmer (40°C) and hypersaline (35-60%) than dome-base pools (PSBL; Extended Data Table 1). The third zone corresponded to the Yellow Lake and neighboring ponds (Fig. 1e, Extended Data Figs. 1d and 2i-k), an acidic (pH~1.8), warm (~40°C) and extremely hypersaline[16] system (≥50%). The Yellow Lake actively bubbles, emitting toxic gases, as attested by numerous dead birds around. The gas phase includes light hydrocarbons[8]. The fourth zone comprised the hypersaline (36%), almost neutral (pH~6.5), Lake Assale (Fig. 1b, Extended Data Fig. 2r), which we used as a milder, yet extreme, Danakil system for comparison. In contrast with a continuous degassing activity, the hydrothermal manifestations were highly dynamic, especially on the dome and the Black Mountain area. Indeed, the area affected by hydrothermal activity in January 2017 was much more extensive than the year before (Fig. 1 and Extended Data Fig. 1). Dallol chimneys and hyperacidic ponds can appear and desiccate in a matter of days or weeks, generating a variety of evaporitic crystalline structures observable in situ[17]. Likewise, very active, occasionally explosive (salt 'bombs'), hydrothermal activity characterized by hot (110°C), slightly acidic (pH~4.4), black hypersaline fluids was detected in the Black Mountain area in 2016 ('Little Dallol'; sample BL6-01; Extended Data Figs. 1b and 2l) but not in the following years. Also, active bischofite flows[6,7,18] (116°C) were observed in the Black Mountain area in 2016 but not in 2017.

To assess potential correlations between microbial life and local chemistry, we analyzed the chemical composition of representative samples used in parallel for microbial diversity analyses (see Methods). Our results revealed three major types of solution chemistry depending on the dominant elements (Fig. 2f; Extended Data Fig. 3a). In agreement with recent observations, Dallol ponds were characterized by NaCl supersaturated brines highly enriched in Fe with different oxidation states, largely explaining color variation[17]. Potassium and sulfur were also abundant (Supplementary Table 1). By contrast, samples from the salt canyons and plain near Dallol and Lake Assale were essentially NaCl-dominated, with much lower Fe content, while the Yellow and Black lakes and associated ponds had very high Mg^{2+} and Ca^{2+}

concentrations (Supplementary Table 1). Many aromatic compounds were identified, especially in Dallol and Yellow Lake fluids (Supplementary Table 2). Because high chaotropicity associated with Mg_2Cl-rich brines, high ionic strength and low water activity (a_w) are thought to be limiting factors for life[12,13,19,20], we determined these parameters in representative samples (Extended Data Table 2). Based on our experimental measures and theoretical calculations from dominant salts, only samples in the Black and Yellow lake areas displayed life-limiting chaotropicity and a_w values according to established limits[12,13,19,20]. A principal component analysis (PCA) showed that the sampled environments were distributed in three major groups depending on solution chemistry, pH and temperature: Black and Yellow Lake samples, anticorrelating with a_w; Dallol dome samples, mostly correlating with a_w but anticorrelating with pH; and Dallol canyon cave reservoir (Gt samples) and Lake Assale, correlating both with a_w and pH (Fig. 2g). These results are consistent with those obtained with ANOVA and subsequent post-hoc analysis, which show significant differences between the majority of the groups among them and for the variables tested (Supplementary Table 4).

To ascertain the occurrence and diversity of microbial life along these physicochemical gradients, we purified DNA from a broad selection of brine samples (0.2-30-µm cell fraction), and solid samples (gypsum and halite-rich salt crusts, compacted sediment and soil-like samples; Extended Data Table 1). We carried out 16S/18S rRNA gene-based diversity studies by high-throughput short-amplicon sequencing (metabarcoding approach) but also sequenced almost-full-length genes from clone libraries, providing local reference sequences for more accurate phylogenetic analyses (see Methods). Despite intensive PCR efforts and extensive sampling in Dallol polyextreme ponds, including pools that were active in two consecutive years (Extended Data Fig. 1) to minimize ephemeral system-derived effects, we only amplified 16S/18S rRNA genes from Dallol canyon cave water, the dome-base geothermally-influenced salt plain and Lake Assale, but never from the Dallol dome and Black/Yellow lakes (Fig. 3a). To check whether this resulted from excessively low DNA amounts in those samples (although relatively large volumes were filtered), we carried out semi-nested PCR reactions using as templates potential amplicons produced during the first PCR-amplification reaction, including first-PCR negative controls. Almost all samples produced amplicons in semi-nested PCR-reactions, including the first-PCR blanks (Fig. 3a). Metabarcoding analysis revealed that amplicons from direct PCR-reactions (PS/PS3, Gt, Assale) were largely dominated by archaeal sequences (>85%), grouping in diverse and abundant OTUs (Extended Data Table 3). By contrast, amplicons derived from Dallol ponds, Black and Yellow lakes but also first-PCR 'negative'-controls were dominated by bacterial sequences. Most of them were related to well-known kit and laboratory contaminants[21,22], other were human-related bacteria likely introduced during intensive

afar and tourist daily visits to the site; a few archaeal sequences might result from aerosol cross-contamination despite extensive laboratory precautions (see Methods). After removal of contaminant sequences (grey bars, Fig. 3a; Supplementary Table 5), only rare OTUs encompassing few reads (mostly archaeal) could be associated to Dallol dome or Yellow Lake brines, which we interpret as likely dispersal forms (dusty wind is frequent in the area). Slightly higher abundances of archaeal OTUs were identified in 'soil' samples, i.e. samples retrieved from salty consolidated mud or crusts where dust brought by the wind from the surrounding plateaus accumulates and starts constituting a proto-soil (with incipient microbial communities; e.g. Extended Data Fig. 2i). Therefore, while we cannot exclude the presence of active life in these 'soil' samples, our results strongly suggest that active microbial life is absent from polyextreme Dallol ponds and the Black and Yellow lakes.

By contrast, PS/PS3, Gt and Assale samples harbored extremely diverse archaea (2,653 OTUs conservatively determined at 95% identity, i.e. genus level) that virtually spanned the known archaeal diversity (Fig. 3; Extended Data Table 3; Supplementary Table 5). Around half of that diversity belonged to Halobacteria, and an additional quarter to the Nanohaloarchaeota[23]. The rest of archaea distributed in lineages typically present in hypersaline environments, e.g. the Methanonatronoarchaeia[24,25] and Candidate Divison MSBL1, thought to encompass methanogens[26] and/or sugar-fermentors[27], but also other archaeal groups not specifically associated with salty systems (although can sometimes be detected in hypersaline settings, e.g. some Thermoplasmata or Woesearchaeota). These included Thermoplasmata and Archaeoglobi within Euryarchaeota, Woesearchaeota and other lineages (Aenigmarchaeota, Altiarchaeales) usually grouped as DPANN[28-30] and Thaumarchaeota and Crenarchaeota (Sulfolobales) within the TACK/Proteoarchaeota[31] (Fig. 3a; Supplementary Table 5). In addition, based on the fact that rRNA GC content correlates with growth temperature, around 27% and 6% of archaeal OTUs were inferred to correspond to, respectively, thermophilic and hyperthermophilic organisms (see Methods; Fig. 3b). As previously observed[23,28,29], common archaeal primers for near-full 16S rRNA genes (Fig. 3c, red dots) failed to amplify Nanohaloarchaeota and other divergent DPANN lineages. These likely encompass ectosymbionts/parasites[28-30,32]. Given their relative abundance and co-occurrence in these and other ecosystems, it is tempting to hypothesize that Nanohaloarchaeota are (ecto)symbionts of Halobacteria; likewise, Woesearchaeota might potentially be associated with *Thermoplasma*-like archaea. Although much less abundant, bacteria belonging to diverse phyla, including CPR (Candidate Phyla Radiation) lineages, were also present in these samples (710 OTUs; Extended Data Fig. 4; Extended Data Table 3; Supplementary Table 5). In addition to typical extreme halophilic genera (e.g. *Salinibacter*, Bacteroidetes), one Deltaproteobacteria group and two divergent bacterial clades were overrepresented in Dallol canyon

Gt samples. Less abundant and diverse, eukaryotes were present in Lake Assale and, occasionally, the salt plain and Gt, being dominated by halophilic *Dunaliella* algae (Extended Data Fig. 5; Supplementary Table 6).

Consistent with metabarcoding results, and despite the use of various culture media and growth conditions mimicking local environments (see Methods), cultural approaches did not yield enrichments for any of the Dallol dome, Black and Yellow lake samples. We easily obtained enrichments from the canyon cave (Gt/7Gt) and salt plain (PS/PS3) samples in most culture media (except on benzoate/hexadecane) and tested conditions (except at 70°C in the dark). However, all attempts to isolate microorganisms at pH<3 from these enrichments also failed. The most acidophilic isolate obtained from serial dilutions (PS3-A1) grew only at 37°C and optimal pH 5.5 (range 3-7). Its 16S rRNA gene was 98.5% identical to that of *Halarchaeum rubridurum* MH1-16-3 (NR_112764), an acidophilic haloarchaeon growing at pH 4.0-6.5[33].

In agreement with metabarcoding and culture-derived observations, multiparametric fluorescence analysis showed no DNA fluorescence above background for Dallol and Yellow Lake samples (Extended Data Fig. 6). Because optical and scanning electron microscopy (SEM) observations suggested that indigenous cells were unusually small, we applied fluorescence-activated cell-sorting (FACS) to samples from the different Dallol environments (Extended Data Table 1), followed by systematic SEM analysis of sorted events. Even though some samples showed no difference in fluorescence after incubation with DNA dyes, we sorted all events above background limit (as defined in Fig. 6a). We only detected cells in Dallol cave water and salt plain samples but not in Dallol dome ponds or Yellow Lake samples (Extended Data Fig. 6). Consistent with this, after DNA purification of FACS-sorted particles, 16S rRNA gene amplicons could only be obtained from different cave and salt plain samples but not from Dallol dome or Yellow Lake samples. Cell counts estimated from FACS for the cave and salt plain samples were low (average 3.1 x 10^4 cells.ml^{-1} and 5.3 x 10^4 cells.ml^{-1} for the cave and PS samples, respectively). Sorted cells were usually small to ultrasmall (down to 0.25-0.3 µm diameter; Fig. 4). In PS samples, some of these small cells formed colonies (Extended Data Fig. 6, Fig. 4c) sometimes surrounded by an exopolymeric matrix cover (Fig. 4h). The presence of cytoplasmic bridges and/or potential cell fusions (Extended Data Fig. 6, Fig. 4c) suggest that they might be archaeal colonies[34].

FACS-sorted fluorescent particles in Dallol pond samples appeared to correspond exclusively to salt crystals or cell-sized amorphous minerals morphologically resembling cells, i.e. biomorphs[35,36] (e.g. Fig. 4d in comparison with Fig. 4c). This prompted us to carry out a more systematic search for abiotic biomorphs

in our samples. SEM observations coupled with chemical mapping by energy dispersive X-ray spectrometry (EDXS) showed a variety of cocci-like biomorph structures of diverse elemental compositions. Many of them were Si biomorphs (Dallol ponds, Yellow and Assale lakes), but we also detected Fe-Al silicates (Gt), S or S-rich biomorphs (Dallol ponds), and Ca or Mg chlorides (Yellow lake, BLPS samples). (Fig. 4; Extended Data Table 4; Supplementary Figs. 1-2). At the same time, we observed Si-encrusted rod-shaped cells in Lake Assale samples (Fig. 4.l). Therefore, silica rounded precipitates represent ultrasmall cell-like biomorphs in samples with no detectable life but contribute to cell encrustment and potential fossilization when life is present.

Our work has three major implications. First, by studying the microbial distribution along gradients of polyextreme conditions in the geothermal area of Dallol and its surroundings in the Danakil Depression, we identify two major physicochemical barriers that prevent life to thrive in the presence of liquid water on the surface of our planet and, potentially, elsewhere[14], despite it is a widely accepted criterion for habitability. Confirming previous studies[12,13,19,20], one such barrier is imposed by high chaotropicity and low a_w, which are associated to high Mg^{2+}-brines in Black and Yellow lake areas. The second barrier seems to be imposed by the hyperacid-hypersaline combinations found in the Dallol dome ponds (pH~0; salt>35%), regardless of temperature. This suggests that molecular adaptations to simultaneous very low-pH and high-salt extremes are incompatible beyond those limits. In principle, more acidic proteins, intracellular K^+ accumulation ('salt-in' strategy) or internal positive membrane potential generated by cations or H^+/cation antiporters serve both acidophilic and halophilic adaptations[37-39]. However, membrane stability/function problems and/or high external Cl^- concentrations inducing H^+ and cation (K^+/Na^+) import and potentially disrupting membrane bioenergetics[38], might be deleterious under these conditions. We cannot exclude other explanations linked to the presence of multiple stressors, such as high metal content or an increased susceptibility to the presence of local chaotropic salts in the Dallol hyperacidic ponds even if measured chaotropicity values are relatively low (-31 to +19 kJ/kg) as compared to the established limit for life (87.3 kJ/kg)[12,13,20] (Extended Data Table 3). Future studies should help to identify the molecular barriers limiting the adaptation of life to this combination of extremes. Second, although extreme environments usually are low-diversity systems, we identify here exceptionally diverse and abundant archaea spanning known major taxa in hypersaline, mildly acidic systems near life-limit conditions. A wide archaeal (and to a lesser extent, bacterial) diversity seems consistent with suggestions that NaCl-dominated brines are not as extreme as previously thought[40] but also with recent observations that the mixing of meteoric and geothermal fluids leads to hyperdiverse communities[41]. Nonetheless, life at high salt requires extensive molecular adaptations[12,13,19,40], which might seem at odds with multiple

independent adaptations to extreme halophily across archaea. Among those adaptations, the intracellular accumulation of K^+ ('salt-in' strategy), accompanied by the corresponding adaptation of intracellular proteins to function under those conditions, has been crucial. Based on the observation that the deepest archaeal branches correspond to (hyper)thermophilic lineages[42] and that non-halophilic hyperthermophilic archaea accumulate high intracellular K^+ (1.1-3M) for protein thermoprotection[43,44] (thermoacidophiles also need K^+ for pH homeostasis[38]), we hypothesize that intracellular K^+ accumulation is an ancestral archaeal trait that has been independently exapted in different taxa for adaptation to hypersaline habitats. Finally, the extensive occurrence of abiotic, mostly Si-rich, biomorphs mimicking the simple shape and size of ultrasmall cells in the hydrothermally-influenced Dallol settings reinforces the equivocal nature of morphological 'microfossils'[35] and calls for the combination of multiple biosignatures before claiming the presence of life on the early Earth and beyond.

Materials and Methods

Sampling and measurement of physicochemical parameters on site. Samples were collected during two field trips carried out in January 2016 and January 2017 (when air temperature rarely exceeded 40-45°C); a few additional samples were collected in January 2018 (Fig. 1; Extended Data Fig. 1 and Extended Data Table 1). All sampling points and mapping data were georeferenced using a Trimble® handheld GPS (Juno SB series) equipped with ESRI software ArcPad® 10. Cartography of hydrogeothermal activity areas was generated using ESRI GIS ArcMap™ mapping software ArcGis® 10.1 over georeferenced Phantom-4 drone images taken by O. Grunewald during field campaigns, compared with and updating previous local geological cartography[7]. Samples were collected in three major areas at the Dallol dome and its vicinity (Fig. 1b): i) the top of the Dallol dome, comprising various hydrothermal pools with diverse degrees of oxidation (Fig.1c); ii) the Black Mountain area (Fig. 1d), including the Black Lake and surrounding bischofite flows and the South-Western salt canyons harboring water reservoirs often influenced by the geothermal activity and iii) the Yellow Lake (Gaet'Ale) area (Fig. 1e). We also collected samples from the hypersaline Lake Assale (Karum), located a few kilometers to the South in the Danakil Depression (Fig. 1b). Physicochemical parameters (Extended Data Table 1) were measured in situ with a YSI Professional Series Plus multiparameter probe (pH, temperature, dissolved oxygen, redox potential) up to 70°C and a Hanna HI93530 temperature probe (working range -200/1,000°C) and a Hanna HI991001 pH probe (working pH range -2.00/16.00) at higher temperatures. Salinity was measured in situ with a

refractometer on 1:10 dilutions in MilliQ water. Brine samples for chemical analyses were collected in 50 ml glass bottles after prefiltration through 0.22 µm pore-diameter filters; bottles were filled to the top and sealed with rubber stoppers to prevent the (further) oxidation of reduced fluids. Solid and water samples for microbial diversity analyses and culturing assays were collected under the most possible aseptic conditions to prevent contamination (gloves, sterile forceps and containers). Samples for culture assays were kept at room temperature. Salts and mineral fragments for DNA-based analyses were conditioned in Falcon tubes and fixed with absolute ethanol. Water samples (volumes for each sample are indicated in Supplementary Table 1) were filtered through 30 µm pore-diameter filters to remove large particles and sequentially filtered either through 0.22 µm pore-diameter filters (Whatman®) or using 0.2 µm pore-size Cell-Trap units (MEM-TEQ Ventures Ltd, Wigan, UK). Filters or Cell-Trap concentrates retaining 0.2-30 µm particles were fixed in 2-ml cryotubes with absolute ethanol (>80% final concentration). Back in the laboratory, ethanol-fixed samples were stored at -20°C until use.

Chemical analyses, salinity, chaotropicity, ionic strength and water activity. The chemical composition of solid and 0.2 µm-prefiltered liquid samples was analyzed at the SIDI service (Universidad Autónoma de Madrid). Major and trace elements in liquid samples were analyzed by total reflection X-ray fluorescence (TXRF) with a TXRF-8030c FEI spectrometer and inductively coupled plasma mass spectrometry (ICP-MS) using a Perkin-Elmer NexION 300XX instrument. Ions were analyzed using a Dionex DX-600 ion chromatography system. Organic molecules were characterized using a Varian HPLC-DAD/FL/LS liquid chromatograph. Crystalline phases in solid samples were characterized by x-ray diffraction using a X'Pert PRO Theta/Theta diffractometer (Panalytical) and identified by comparison with the International Centre for Diffraction Data (ICDD) PDF-4+ database using the 'High Score Plus' software (Malvern Panalytical https://www.malvernpanalytical.com/es/products/category/software/x-ray-diffraction-software/highscore-with-plus-option). Inorganic data are provided in Supplementary Table 1; organic and ionic chemistry data in Supplementary Tables 2 and 3, respectively. Salinity (weight/volume) was also experimentally measured in triplicates (and up to 6 replicates) by weighting the total solids after heat-drying 1 ml aliquots in ceramic crucibles at 120°C for at least 24h. Chaotropicity was experimentally measured according to the temperature of gelation of ultrapure gelatin (for Ca-rich samples) and agar (rest of samples) determined using the spectrometric assay developed by Cray et al.[45] (Extended Data Table 2). Chaotropicity was also calculated according to Cray and coworkers[46] based on the abundance of dominant Na, K, Mg, Ca and Fe cations and, on the ground that Cl is the dominant anion, assuming they essentially form chlorine salts (NaCl, KCl, $MgCl_2$, $CaCl_2$ and $FeCl_2$). Ionic strength was calculated according

to Fox-Powell et al.[47]. Water activity was measured on 10-ml unfiltered aliquots at room temperature (25°C) using a HC2-AW probe and HP23-AW-A indicator (Rotronic AG, Bassersdorf, Switzerland) calibrated at 23°C using the AwQuick acquisition mode (error per measure 0.0027). From a strict biological perspective, these water activity measurements are not precise enough and need to be considered as indicative, since cells can be sensitive to a 0.001 water-activity change[48]. They follow, however, the same trend as shown by the other related parameters measured experimentally (salinity, chaotropicity). Principal component analyses (PCA) of samples, chemical and physicochemical parameters (Fig. 2 and Extended Data Fig. 3) were done using R-software[49] packages FactoMineR[50] and factoextra[51]. Differences between the groups of samples belonging to the same physicochemical zone segregating in the PCA were tested using the one-way ANOVA module of IBM SPSS Statistics 24 software. The significance of differences among groups and with the measured parameters were checked by means of a post-hoc comparison using the Bonferroni test.

DNA purification and 16/18S rRNA gene metabarcoding. DNA from filters, Cell-Trap concentrates and grinded solid samples was purified using the Power Soil DNA Isolation Kit (MoBio, Carlsbad, CA, USA) under a UV-irradiated Erlab CaptairBio DNA/RNA PCR Workstation. Prior to DNA purification, filters were cut in small pieces with a sterile scalpel and ethanol remaining in cryotubes filtered through 0.2 µm pore-diameter filters and processed in the same way. Ethanol-fixed Cell-Trap concentrates were centrifuged for 10 min at 13,000 rpm and the pellet resuspended in the first kit buffer. Samples were let rehydrate for at least 2h at 4°C in the kit resuspension buffer. For a selection of Cell-Trap concentrates, FACS-sorted cells and to monitor potential culture enrichments, we also used the Arcturus PicoPure DNA Isolation kit (Applied Biosystems – Foster City, CA, USA; samples labeled pp). DNA was resuspended in 10 mM Tris-HCl, pH 8.0 and stored at -20°C. Bacterial and archaeal 16S rRNA gene fragments of approximatively 290 bp encompassing the V4 hypervariable region were PCR-amplified using U515F (5'-GTGCCAGCMGCCGCGGTAA) and U806R (5'-GGACTACVSGGGTATCTAAT) primers. PCR reactions were conducted in 25 µl, using 1.5 mM $MgCl_2$, 0.2 mM of each dNTP (PCR Nucleotide Mix, Promega), 0.1 µM of each primer, 1 to 5 µl of purified 'DNA' and 1 U of the hot-start Taq Platinum polymerase (Invitrogen, Carlsbad, CA, USA). GoTaq (Promega) was also tried when amplicons were not detected but did not yield better results. Amplification reactions proceeded for 35 cycles (94°C for 15 s, 50 to 55°C for 30 s and 72°C for 90 s), after a 2 min-denaturation step at 94°C and before a final extension at 72°C for 10 min. Amplicons were visualized after gel electrophoresis and ultrasensitive GelRed® nucleic acid gel stain

(Biotium, Fremont, CA, USA) on a UV-light transilluminator. When direct PCR reactions failed to yield amplicons after several assays, PCR conditions and using increasing amounts of input potential DNA, semi-nested reactions using those primers were carried out using as template 1 µl of PCR products, including negative controls, from a first amplification reaction done with universal prokaryotic primers U340F (5'-CCTACGGGRBGCASCAG) and U806R. Eukaryotic 18S rRNA gene fragments including the V4 hypervariable region were amplified using primers EK-565F (5'-GCAGTTAAAAAGCTCGTAGT) and 18S-EUK-1134-R-UNonMet (5'-TTTAAGTTTCAGCCTTGCG). Primers were tagged with different Molecular IDentifiers (MIDs) to allow multiplexing and subsequent sequence sorting. Amplicons from at least 5 independent PCR products for each sample were pooled together and then purified using the QIAquick PCR purification kit (Qiagen, Hilden, Germany). Whenever semi-nested PCR reactions yielded amplicons, semi-nested reactions using as input first-PCR negative controls also yielded amplicons (second-PCR controls did not yield amplicons). Products of these positive 'negative' controls were pooled in two control sets (1 and 2) and sequenced along with the rest of amplicons. DNA concentrations were measured using Qubit™ dsDNA HS assays (Invitrogen). Equivalent amplicon amounts obtained for 54 samples (including controls) were multiplexed and sequenced using paired-end (2x300 bp) MiSeq Illumina technology (Eurofins Genomics, Ebersberg, Germany). In parallel, we tried to amplify near-complete 16S/18S rRNA gene fragments (~1400-1500 bp) using combinations of forward archaea-specific primers (21F, 5'-TTCCGGTTGATCCTGCCGGA; Ar109F, 5'-ACKGCTGCTCAGTAACACGT) and bacteria-specific primers (27F, 5'-AGAGTTTGATCCTGGCTCAG) with the prokaryotic reverse primer 1492R (5'-GGTTACCTTGTTACGACTT) and eukaryotic primers 82F (5'-GAAACTGCGAATGGCTC) and 1520R (5'-CYGCAGGTTCACCTAC). When amplified, DNA fragments were cloned using TopoTA™ cloning (Invitrogen) and clone inserts were Sanger-sequenced to yield longer reference sequences. Forward and reverse Sanger sequences were quality-controlled and merged using Codon Code Aligner (http://www.codoncode.com/aligner/).

Sequence treatment and phylogenetic analyses. Paired-end reads were merged and treated using a combination of existing software to check quality, eliminate primers and MIDs and eliminate potential chimeras. Sequence statistics are given in Extended Data Table 3. Briefly, read merging was done with FLASH[52], primers and MIDs trimmed with cutadapt[53] and clean merged reads dereplicated using vsearch[54], with the uchime_denovo option to eliminate potential chimeras. The resulting dereplicated clean merged reads were used then to define operational taxonomic units (OTUs) at 95% identity cut-off using CD-HIT-EST[55]. This cut-off offered i) a reasonable operational approximation to the genus level diversity while producing a manageable number of OTUs to be included in phylogenetic trees (see below)

and ii) allowed us a conservative identification of potential contaminants in our semi-nested PCR-derived datasets. Diversity (Simpson), richness (Chao1) and evenness indices were determined using R-package "vegan" (Supplementary Table 5). OTUs were assigned to known taxonomic groups based on similarity with sequences of a local database including sequences from cultured organisms and environmental surveys retrieved from SILVAv128[56] and PR2v4[57]. The taxonomic assignation of bacteria and archaea was refined by phylogenetic placement of OTU representative sequences in reference phylogenetic trees. To build these trees, we produced, using Mafft-linsi v7.38[58], alignments of near full-length archaeal and bacterial 16S rRNA gene sequences comprising Sanger sequences from our gene libraries (144 archaeal, 91 bacterial) and selected references for major identified taxa plus the closest blast-hits to our OTUs (702 archaea, 2,922 bacterial). Poorly aligned regions were removed using TrimAl[59]. Maximum likelihood phylogenetic trees were constructed with IQ-TREE[60] using the GTR model of sequence evolution with a gamma law and taking into account invariable sites (GTR+G+I). Node support was estimated by ultrafast bootstrapping as implemented in IQ-TREE. Shorter OTU representative sequences (2,653 archaeal, 710 bacterial) were then added to the reference alignment using MAFFT (accurate -linsi 'addfragments' option). This final alignment was split in two files (references and OTUs) before using the EPA-ng tool (https://github.com/Pbdas/epa-ng) to place OTUs in the reference trees reconstructed with IQ-TREE. The jplace files generated by EPA-ng were transformed into newick tree files with the genesis library (https://github.com/lczech/genesis). Tree visualization and ring addition were done with GraphLan[61]. To see whether our OTUs might correspond to thermophilic species, we first plotted the GC content of the 16S rRNA gene region used for metabarcoding analyses of a selection of 88 described archaeal species with optimal growth temperatures ranging from 15 to 103°C. These included representatives of all Halobacteria genera, since they are often characterized by high GC content. A regression analysis confirmed the occurrence of a positive correlation[62] between rRNA GC content and optimal growth temperature also for this shorter 16S rRNA gene amplified region (Fig. 3b). We then plotted the GC content of our archaeal OTUs on the same graph. Dots corresponding to Halobacteria genera remain out of the dark shadowed area in Fig. 3b.

Cultures. Parallel culture attempts were carried out in two different laboratories (Orsay and Madrid). We used several culture media derived from a classical halophile's base mineral growth medium[63] containing (gl^{-1}): NaCl (234), KCl (6), NH_4Cl (0.5), K_2HPO_4 (0.5), $(NH_4)_2SO_4$ (1), $MgSO_4.7H_2O$ (30.5), $MnCl_2.7H_2O$ (19.5), $CaCl_2.6H_2O$ (1.1) and Na_2CO_3 (0.2). pH was adjusted to 4 and 2 with 10N H_2SO_4. The autoclaved medium was amended with filter-sterilized cyanocobalamin (1 µM final concentration) and 5 ml of an autoclaved

385 $CaCl_2.6H_2O$ 1M stock solution. Medium MDH2 contained yeast extract (1 gl^{-1}) and glucose (0.5 gl^{-1}). Medium MDSH1 had only 2/3 of each base medium salt concentration plus $FeCl_3$ (0.1 gl^{-1}) and 10 $ml.l^{-1}$ of Allen´s trace solution. It was supplemented with three energy sources (prepared in 10 ml distilled water at pH2 and sterilized by filtration): yeast extract (1 gl^{-1}) and glucose (0.5 gl^{-1}) (MDS1-org medium); $Na_2S_2O_3$ (5 gl^{-1}) (MDS1-thio medium) and $FeSO_4.7H_2O$ (30 gl^{-1}) (MDS1-Fe medium). Medium MDSH2 mimicked 390 more closely some Dallol salts as it also contained (gl^{-1}): $FeCl_3$ (0.1), $MnCl_2.4H_2O$ (0.7), $CuSO_4$ (0.02), $ZnSO_4.7H_2O$ (0.05) and LiCl (0.2) as well as 10 ml l^{-1} of Allen´s trace solution combined with the same energy sources used for MDSH1, yielding media MDSH2-org, MDSH2-thio and MDSH2-Fe. For enrichment cultures, we added 0.1 ml liquid samples to 5 ml medium at pH 2 and 4 and incubated at 37, 50 and 70°C in 10-ml sterile glass tubes depending on the original sample temperatures. Three additional variants of 395 the base salt medium supplemented with $FeCl_3$ and trace minerals contained 0.2 gl^{-1} yeast extract (SALT-YE), 0.5 gl^{-1} thiosulfate (SALT-THIO) or 0.6 gl^{-1} benzoate and 5 mM hexadecane (SALT-BH). The pH of these media was adjusted with 34% HCl to 1.5 for Dallol and Black Lake samples, and to 3.5 for YL, PS3 and PSBL samples. 1 ml of sample was added to 4 ml of medium and incubated at 45°C in a light regime and at 37°C and 70°C in the dark. We also tried cultures in anaerobic conditions. Potential growth was monitored by 400 optical microscopy and, for some samples, SEM. In the rare cases where enrichments were obtained, we attempted isolation by serial dilutions.

Flow cytometry and fluorescence-activated cell sorting (FACS). The presence of cell/particle populations above background level in Dallol samples was assessed with a flow-cytometer cell-sorter FACSAria™III 405 (Becton Dickinson). Several DNA dyes were tested for lowest background signal in forward scatter (FSC) red (695±20 nm) and green (530±15 nm) fluorescence (Extended Data Fig. 6a) using sterile SALT-YE medium as blank. DRAQ5™ and SYTO13® (ThermoFisher) were retained and used at 5 µM final concentration to stain samples in the dark at room temperature for 1 h. Cell-Trap concentrated samples were diluted at 20% with 0.1-µm filtered and autoclaved MilliQ® water. The FACSAria™III was set at 410 purity sort mode triggering on the forward scatter (FSC). Fluorescent target cells/particles were gated based on the FSC and red or green fluorescence (Extended Data Fig. 6b) and flow-sorted at a rate of 1-1,000 particles per second. Sorting was conducted using the FACSDiva™ software (Becton Dickinson); figures were done with the FCSExpress 6 software (De Novo Software). Sorted cells/particles were subsequently observed by scanning electron microscopy for characterization. Minimum and maximum 415 cell abundances were estimated based on the number of sorted particles, duration of sorting and minimal (10µl min-1) and maximal (80µl min-1) flow rates of the FACSAria (Becton Dickinson FACSAria manual).

Scanning electron microscopy (SEM) and elemental analysis. SEM analyses were carried out on natural samples, FACS-sorted cells/particles and a selection of culture attempts. Liquid samples were deposited on top of 0.1 µm pore-diameter filters (Whatman®) under a mild vacuum aspiration regime and briefly rinsed with 0.1-µm filtered and autoclaved MilliQ® water under the same vacuum regime. Filters were let dry and sputtered with carbon prior to SEM observations. SEM analyses were performed using a Zeiss ultra55 field emission gun (FEG) SEM. Secondary electron (SE2) images were acquired using an In Lens detector at an accelerating voltage of 2.0 kV and a working distance of ~7.5 mm. Backscattered electron images were acquired for chemical mapping using an angle selective backscattered (AsB) detector at an accelerating voltage of 15 kV and a working distance of ~7.5 mm. Elemental maps were generated from hyperspectral images (HyperMap) by energy dispersive X-ray spectrometry (EDXS) using an EDS QUANTAX detector. EDXS data were analyzed using the ESPRIT software package (Bruker).

Data availability

Sanger sequences have been deposited in GenBank (NCBI) with accession numbers MK894601-MK894820 and Illumina sequences in GenBank Short Read Archive with BioProject number PRJNA541281.

References

1 Harrison, J. P., Gheeraert, N., Tsigelnitskiy, D. & Cockell, C. S. The limits for life under multiple extremes. *Trends Microbiol* **21**, 204-212 (2013).

2 Merino, N. *et al.* Living at the extremes: Extremophiles and the limits of life in a planetary context. *Frontiers in Microbiology* **10** (2019).

3 Johnson, S. S., Chevrette, M. G., Ehlmann, B. L. & Benison, K. C. Insights from the metagenome of an acid salt lake: the role of biology in an extreme depositional environment. *PLoS One* **10**, e0122869 (2015).

4 Zaikova, E., Benison, K. C., Mormile, M. R. & Johnson, S. S. Microbial communities and their predicted metabolic functions in a desiccating acid salt lake. *Extremophiles* **22**, 367-379 (2018).

5 Futterer, O. *et al.* Genome sequence of *Picrophilus torridus* and its implications for life around pH 0. *Proc Natl Acad Sci U S A* **101**, 9091-9096 (2004).

6 Varet, J. in *Geology of Afar (East Africa). Regional Geology Reviews* (eds R. Oberhänsli, M. J. de Wit, & F. M. Roure) Ch. 7, 205-226 (Springer, 2018).

7 Franzson, H., Helgadóttir, H. M. & Óskarsson, F. in *Proceedings World Geothermal Congress.* 11.

8 Darrah, T. H. *et al.* Gas chemistry of the Dallol region of the Danakil Depression in the Afar region of the northern-most East African Rift. *Chemical Geology* **339**, 16-29 (2013).

9 Holwerda, J. G. & Hutchinson, R. W. Potash-bearing evaporites in the Danakil area, Ethiopia. *Economic Geology* **63**, 124-150 (1968).

10 Warren, J. K. Danakhil potash, Ethiopia: Beds of kainite/carnallite, Part 2 of 4. (2015).

11 Cavalazzi, B. *et al.* The Dallol geothermal area, Northern Afar (Ethiopia)-An exceptional planetary field analog on Earth. *Astrobiology* **19**, 553-578 (2019).

12 Hallsworth, J. E. *et al.* Limits of life in $MgCl_2$-containing environments: chaotropicity defines the window. *Environ Microbiol* **9**, 801-813 (2007).

13 Stevenson, A. *et al.* Is there a common water-activity limit for the three domains of life? *ISME J* **9**, 1333-1351 (2015).

14 McKay, C. P. Requirements and limits for life in the context of exoplanets. *Proc Natl Acad Sci U S A* **111**, 12628-12633 (2014).

15 Moissl-Eichinger, C., Cockell, C. & Rettberg, P. Venturing into new realms? Microorganisms in space. *FEMS Microbiol Rev* **40**, 722-737 (2016).

16 Pérez, E. & Chebude, Y. Chemical analysis of Gaet'ale, a hypersaline pond in Danakil Depression (Ethiopia): New record for the most saline water body on Earth. *Aquat Geochem* **23**, 109–117 (2017).

17 Kotopoulou, E. *et al.* A polyextreme hydrothermal system controlled by iron: The case of Dallol at the Afar Triangle. *ACS Earth Space Chem* **3**, 90-99 (2019).

18 Warren, J. K. Danakhil Potash, Ethiopia: Is the present geology the key? Part 1 of 4. (2015).

19 Tosca, N. J., Knoll, A. H. & McLennan, S. M. Water activity and the challenge for life on early Mars. *Science* **320**, 1204-1207 (2008).

20 Stevenson, A. *et al. Aspergillus penicillioides* differentiation and cell division at 0.585 water activity. *Environ Microbiol* **19**, 687-697 (2017).

21 Sheik, C. S. *et al.* Identification and removal of contaminant sequences from ribosomal gene databases: Lessons from the Census of Deep Life. *Front Microbiol* **9**, 840 (2018).

22 Weyrich, L. S. *et al.* Laboratory contamination over time during low-biomass sample analysis. *Mol Ecol Resour* **19**, 982-996 (2019).

23 Narasingarao, P. *et al.* De novo metagenomic assembly reveals abundant novel major lineage of Archaea in hypersaline microbial communities. *ISME J* **6**, 81-93 (2012).

24 Sorokin, D. Y. *et al.* Discovery of extremely halophilic, methyl-reducing euryarchaea provides insights into the evolutionary origin of methanogenesis. *Nat Microbiol* **2**, 17081 (2017).

25 Sorokin, D. Y. *et al.* Methanonatronarchaeum thermophilum gen. nov., sp. nov. and 'Candidatus Methanohalarchaeum thermophilum', extremely halo(natrono)philic methyl-reducing methanogens from hypersaline lakes comprising a new euryarchaeal class Methanonatronarchaeia classis nov. *Int J Syst Evol Microbiol* **68**, 2199-2208 (2018).

26 Borin, S. *et al.* Sulfur cycling and methanogenesis primarily drive microbial colonization of the highly sulfidic Urania deep hypersaline basin. *Proc Natl Acad Sci U S A* **106**, 9151-9156 (2009).

27 Mwirichia, R. *et al.* Metabolic traits of an uncultured archaeal lineage--MSBL1--from brine pools of the Red Sea. *Sci Rep* **6**, 19181 (2016).

28 Castelle, C. J. *et al.* Biosynthetic capacity, metabolic variety and unusual biology in the CPR and DPANN radiations. *Nat Rev Microbiol* **16**, 629-645 (2018).

29 Castelle, C. J. & Banfield, J. F. Major new microbial groups expand diversity and alter our understanding of the Tree of Life. *Cell* **172**, 1181-1197 (2018).

30 Dombrowski, N., Lee, J. H., Williams, T. A., Offre, P. & Spang, A. Genomic diversity, lifestyles and evolutionary origins of DPANN archaea. *FEMS Microbiol Lett* **366**, fnz008 (2019).

31 Petitjean, C., Deschamps, P., Lopez-Garcia, P. & Moreira, D. Rooting the domain archaea by phylogenomic analysis supports the foundation of the new kingdom proteoarchaeota. *Genome Biol Evol* **7**, 191-204 (2014).

32 Golyshina, O. V. *et al.* 'ARMAN' archaea depend on association with euryarchaeal host in culture and in situ. *Nat Commun* **8**, 60 (2017).

33 Minegishi, H. *et al.* Acidophilic haloarchaeal strains are isolated from various solar salts. *Saline Systems* **4**, 16 (2008).

34 Naor, A. & Gophna, U. Cell fusion and hybrids in Archaea: prospects for genome shuffling and accelerated strain development for biotechnology. *Bioengineered* **4**, 126-129 (2013).

35 Garcia-Ruiz, J. M. *et al.* Self-assembled silica-carbonate structures and detection of ancient microfossils. *Science* **302**, 1194-1197 (2003).

36 Garcia-Ruiz, J. M., Melero-Garcia, E. & Hyde, S. T. Morphogenesis of self-assembled nanocrystalline materials of barium carbonate and silica. *Science* **323**, 362-365 (2009).

37 Slonczewski, J. L., Fujisawa, M., Dopson, M. & Krulwich, T. A. Cytoplasmic pH measurement and homeostasis in bacteria and archaea. *Adv Microb Physiol* **55**, 1-79 (2009).

38 Buetti-Dinh, A., Dethlefsen, O., Friedman, R. & Dopson, M. Transcriptomic analysis reveals how a lack of potassium ions increases Sulfolobus acidocaldarius sensitivity to pH changes. *Microbiology* **162**, 1422-1434 (2016).

39 Gunde-Cimerman, N., Plemenitas, A. & Oren, A. Strategies of adaptation of microorganisms of the three domains of life to high salt concentrations. *FEMS Microbiol Rev* **42**, 353-375 (2018).

40 Lee, C. J. D. *et al.* NaCl-saturated brines are thermodynamically moderate, rather than extreme, microbial habitats. *FEMS Microbiol Rev* **42**, 672-693 (2018).

41 Colman, D. R., Lindsay, M. R. & Boyd, E. S. Mixing of meteoric and geothermal fluids supports hyperdiverse chemosynthetic hydrothermal communities. *Nat Commun* **10**, 681 (2019).

42 López-García, P., Zivanovic, Y., Deschamps, P. & Moreira, D. Bacterial gene import and mesophilic adaptation in archaea. *Nat Rev Microbiol* **13**, 447-456 (2015).

43 Hensel, R. & König, H. Thermoadaptation of methanogenic bacteria by intracellular ion concentration. *FEMS Microbiology Letters* **49**, 75-79 (1988).

44 Shima, S., Thauer, R. K. & Ermler, U. Hyperthermophilic and salt-dependent formyltransferase from Methanopyrus kandleri. *Biochem Soc Trans* **32**, 269-272 (2004).

45 Cray, J. A., Russell, J. T., Timson, D. J., Singhal, R. S. & Hallsworth, J. E. A universal measure of chaotropicity and kosmotropicity. *Environ Microbiol* **15**, 287-296 (2013).

46 Cray, J. A. *et al.* Chaotropicity: a key factor in product tolerance of biofuel-producing microorganisms. *Curr Opin Biotechnol* **33**, 228-259 (2015).

47 Fox-Powell, M. G., Hallsworth, J. E., Cousins, C. R. & Cockell, C. S. Ionic strength is a barrier to the habitability of Mars. *Astrobiology* **16**, 427-442 (2016).

48 Stevenson, A. *et al.* Multiplication of microbes below 0.690 water activity: implications for terrestrial and extraterrestrial life. *Environ Microbiol* **17**, 257-277 (2015).

49 R: A language and environment for statistical computing. v. http://www.r-project.org (R Foundation for Statistical Computing, Vienna, Austria, 2017).

50 Lê, S., Josse, J. & Husson, F. FactoMineR: An R package for multivariate analysis. *Journal of Statistical Software* **25**, 1-18 (2008).

51 factoextra: Extract and visualize the results of multivariate data analyses (https://CRAN.R-project.org/package=factoextra, 2017).

52 Magoc, T. & Salzberg, S. L. FLASH: fast length adjustment of short reads to improve genome assemblies. *Bioinformatics* **27**, 2957-2963 (2011).

53 Martin, M. Cutadapt removes adapter sequences from high-throughput sequencing reads. *EMBnet.Journal* **17**, 10-12 (2011).

54 Rognes, T., Flouri, T., Nichols, B., Quince, C. & Mahe, F. VSEARCH: a versatile open source tool for metagenomics. *PeerJ* **4**, e2584 (2016).

55 Fu, L., Niu, B., Zhu, Z., Wu, S. & Li, W. CD-HIT: accelerated for clustering the next-generation sequencing data. *Bioinformatics* **28**, 3150-3152 (2012).

56 Quast, C. *et al.* The SILVA ribosomal RNA gene database project: improved data processing and web-based tools. *Nucleic Acids Res* **41**, D590-D596 (2013).

57 Guillou, L. *et al.* The Protist Ribosomal Reference database (PR2): a catalog of unicellular eukaryote Small Sub-Unit rRNA sequences with curated taxonomy. *Nucleic Acids Res* **41**, D597-D604 (2013).

58 Katoh, K. & Standley, D. M. MAFFT multiple sequence alignment software version 7: improvements in performance and usability. *Mol Biol Evol* **30**, 772-780 (2013).

59 Capella-Gutierrez, S., Silla-Martinez, J. M. & Gabaldon, T. trimAl: a tool for automated alignment trimming in large-scale phylogenetic analyses. *Bioinformatics* **25**, 1972-1973 (2009).

60 Nguyen, L. T., Schmidt, H. A., von Haeseler, A. & Minh, B. Q. IQ-TREE: a fast and effective stochastic algorithm for estimating maximum-likelihood phylogenies. *Mol Biol Evol* **32**, 268-274 (2015).

61 Asnicar, F., Weingart, G., Tickle, T. L., Huttenhower, C. & Segata, N. Compact graphical representation of phylogenetic data and metadata with GraPhlAn. *PeerJ* **3**, e1029 (2015).

62 Wang, H. C., Xia, X. & Hickey, D. Thermal adaptation of the small subunit ribosomal RNA gene: a comparative study. *J Mol Evol* **63**, 120-126 (2006).

63 Rodriguez-Valera, F., Ruiz-Berraquero, F. & Ramos-Cormenzana, A. Behaviour of mixed populations of halophilic bacteria in continuous cultures. *Can J Microbiol* **26**, 1259-1263 (1980).

Acknowledgments

We are grateful to Olivier Grunewald for co-organizing the Dallol expeditions, documenting field research and providing drone images and to Jean-Marie Hullot (in memoriam), Françoise Brenckmann and the Fondation Iris for funding the first field trip. We thank Luigi Cantamessa for the in situ logistics and discussions about local history. We acknowledge Dr. Makonen Tafari (Mekelle University), Abdul Ahmed Aliyu and the Afar authorities for local assistance as well as the Ethiopian army and the Afar police for providing security. We thank Jacques Barthélémy, Elektra Kotopoulou and Juanma Garcia-Ruiz for help and discussions during field trips. We thank Hélène Timpano and the UNICELL platform for cell sorting, Ana Gutiérrez-Preciado for bioinformatic assistance, Adrienne Kish and Charly Faveau for allowing us to measure water activity of selected samples at the Muséum National d'Histoire Naturelle, Eric Viollier for discussion on chemical analyses, Corentin Gille for help with cultures, Georis Billo for script help to treat SEM pictures and Juan Traba Díaz and Pablo Tejedo Sanz for advice on statistical analyses. This research was funded by the CNRS basic annual funding, the CNRS program TELLUS INTERRVIE and the European Research Council under the European Union's Seventh Framework Program (ERC Grant Agreement 322669). We thank the European COST Action TD1308 'Origins' for funding a short stay of A.L.A. in Orsay. J.B. was financed by the French Ministry of National Education, Research and Technology.

Author contributions

P.L.G. and D.M. designed and supervised the research. P.L.G. organized the scientific expeditions. J.B., P.L.G., D.M., L.J. and J.M.L.G. collected samples and took measurements in situ. J.B., PL.G. and P.B. carried out molecular biology analyses. J.B., A.L.A. and D.M. performed culture, chemistry analyses and water-salt-related measurements. A.L.A. and J.B. performed statistical analyses. J.B., G.R. and D.M. analyzed metabarcoding data. K.B. performed SEM and EDX analyses. J.M.L.G. mapped geothermal activity and georeferenced all samples. L.J. and J.B. performed FACS-derived analyses. P.L.G. and J.B. wrote the manuscript. All authors read and commented on the manuscript.

Competing interests

Authors declare no competing interests.

595 Figure legends

Fig. 1 | Overview of sampling sites at the polyextreme geothermal field of Dallol and its surroundings in the Danakil Depression, Ethiopia. **a**, Location of the Dallol dome area in the Danakil Depression following the alignment of the Erta Ale volcanic range (Gada Ale, Alu-Dalafilla), Northern Ethiopia; **b**, closer view of the sampling zones in the Dallol area and Lake Assale or Karum (satellite image from Copernicus Sentinel 1;
600 2017, January 19th); **c-e**, geological maps showing the sampling sites at (**c**) the Dallol dome summit, (**d**) West salt canyons and Black Mountain, including the Black Lake and (**e**) Yellow Lake (Gaet'Ale) zone. Squares and circles indicate the nature of collected samples and their color, the collection date. The size of circles is proportional to the collected brine volume for analyses. Specific sample names are indicated in the aerial view shown in Extended Data Fig. 1.

605 **Fig. 2 | Physicochemical features of liquid samples from the Dallol area**. **a**, overview of the color palette showed by samples analyzed in this study, reflecting different chemistries and oxidation states; **b-e**, examples of salt-oversaturated samples; **b**, immediate (seconds) precipitation of halite crystals as water from a hot spring (108°C) cools down upon collection; **c-e**, salt precipitates forming after storage at ca. 8°C in water collected from (**c**) Dallol hyperacidic ponds, (**d**) Yellow Lake and (**e**) Black Lake; **f**, Principal
610 Component Analysis (PCA) of 29 samples according to their chemical composition (see Supplementary Table 2). Transition metals group Cr, Mo, Mn, Sc, Zn, V, U, Ce, La, Cu; semimetals, As, B, Sb, Si; basic metals, Tl, Al, Ga, Sh; and alkali metals, Rb, Cs. Some elements are highlighted out of these groups owing to their high relative abundance or to their distant placement. A PCA showing all individual metal variables can be seen in Supplementary Fig. 3a. **g**, PCA of 21samples and key potentially life-limiting
615 physicochemical parameters in the Dallol area (temperature, pH, salinity (TS), water activity). Water activity and salinity-related parameters are provided in Extended Data Table 2. Colored zones in PCA analyses highlight the clusters of samples; they correspond to the three major chemical zones identified in this study.

Fig. 3 | Distribution and diversity of prokaryotes in samples from the Dallol mound and surrounding areas
620 **based on 16S rRNA gene metabarcoding data. a**, histograms showing the presence/absence and abundance of amplicon reads of archaea (upper panel) and bacteria (lower panel) obtained with universal prokaryotic primers. Samples yielding amplicons directly (negative PCR controls were negative) are shown on the right (Direct). Samples for which amplicons were only obtained after nested PCR, all of which also yielded amplicons in 'negative' controls, are displayed on the left (Nested PCR). Sequences identified in

the 'negative' controls, considered as contaminants, are shaded in light grey in the corresponding Dallol samples. The phylogenetic affiliation of dominant archaeal and bacterial groups is color-coded. For details, see Supplementary Table 5. **b**, GC content of archaeal OTUs plotted on a graph showing the positive correlation of GC content (for the same 16S rRNA region) and growth temperature of diverse described archaeal species. **c**, phylogenetic tree of archaeal 16S rRNA gene sequences showing the phylogenetic placement of archaeal OTUs identified in the different environmental samples (full tree provided as Supplementary Data 1). Sequences derived from metabarcoding studies are represented with blue branches (Illumina sequences); those derived from cloning and Sanger sequencing of environmental samples, cultures and FACS-sorted cells are labelled with a red dot. Reference sequences are in black. Concentric circles around the tree indicate the presence/absence of the corresponding OTUs in different groups of samples (groups shown in panel a).

Fig. 4 | Scanning electron microscopy (SEM) pictures and chemical maps of cells and abiotic biomorphs identified in samples from the Dallol region. **a-h**, SEM pictures of cells (**a-c, e-h**) and abiotic biomorphs (**d**). **i-o**, SEM images and associated chemical maps of cells and biomorphs; color intensity provides semi-quantitative information of the mapped elements. **a**, FACS-sorted dividing cells from sample PS (hydrated salt pan between the Dallol dome base and the Black Lake); **b**, FACS-sorted ultrasmall cells from 7Gt samples (cave water reservoir, Dallol canyons); **c**, FACS-sorted colony of ultrasmall cells from sample PS (note cytoplasmic bridges between cells); **d**, FACS-sorted abiotic silica biomorphs from the Dallol pond 7DA9 (note the similar shape and morphology as compared to cells in panel c); **e**, cocci and halite crystals in 8Gt samples (cave water); **f**, long rod in 8Gt; **g**, FACS-sorted cells from Gt samples; **h**, FACS-sorted colonies from sample PS (note the bridge between one naked colony and one colony covered by an exopolymeric-like matrix); **i**, small cocci and amorphous Al-Mg-Fe-rich silicate minerals from Gt; **j**, NaCl crystals and S-Si-rich abiotic biomorphs from Dallol pond sample 7DA7; **k**, NaCl crystal and Si-biomorphs and **l**, Si-encrusted cell and Si-biomorphs in sample 8Ass (Lake Assale); **m**, Mg-Cl biomorph in sample BLPS_04 (Black Lake area pond); **n**, S-rich biomorphs in Dallol pond 7DA9; **o**, Ca-Mg-Cl biomorph in YL-w2 (Yellow Lake pond). SEM photographs were taken using In Lens or AsB detectors; AsB was used for chemical mapping purposes. For additional images and SEM details, see Supplementary Figs. 1-2. White arrows indicate cells difficult to recognize due to their small size and/or flattened aspect possibly resulting

from sample preparation and/or high vacuum conditions within the SEM. The scale bar corresponds to 1 µm.

655

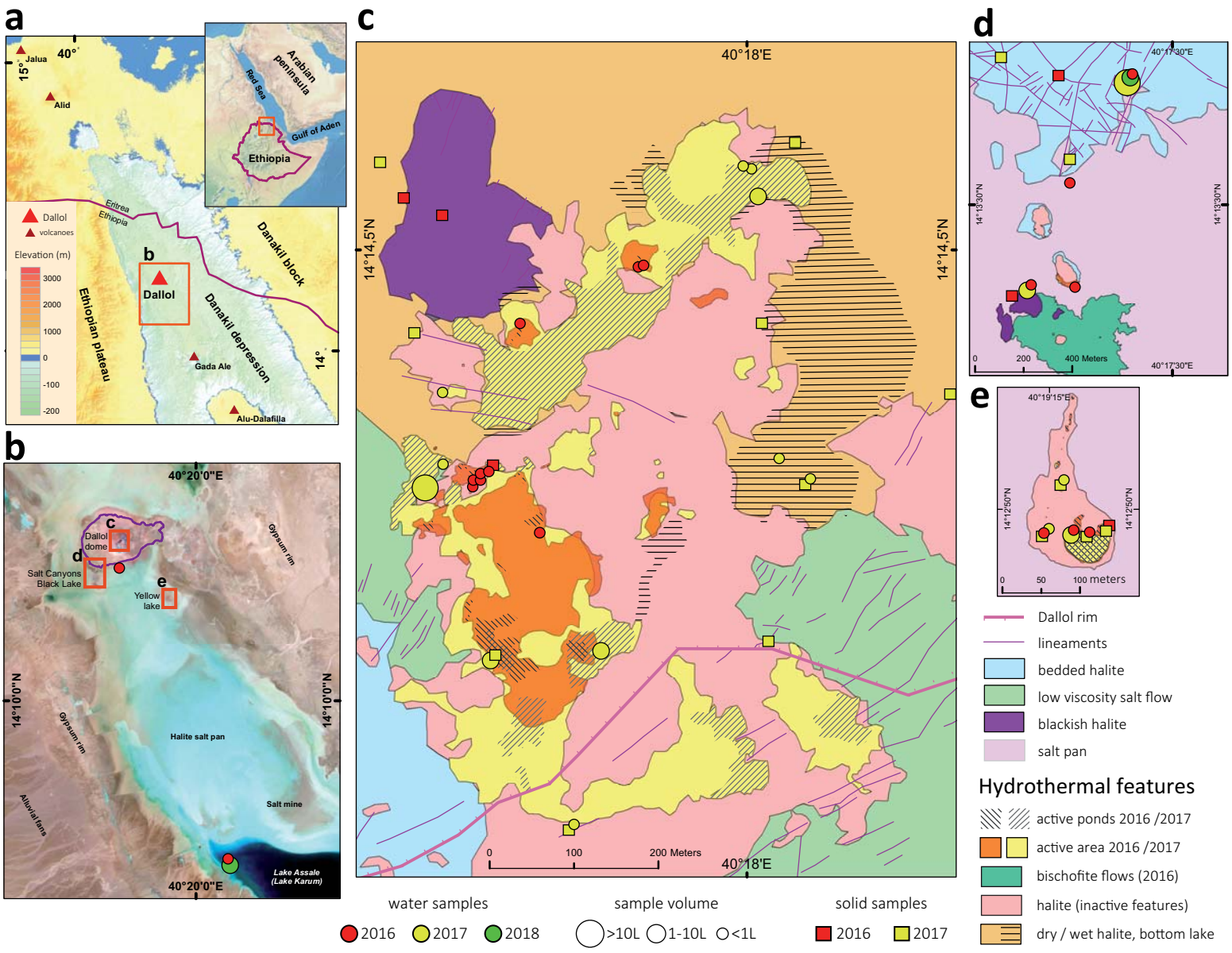

Figure 1. Belilla et al.

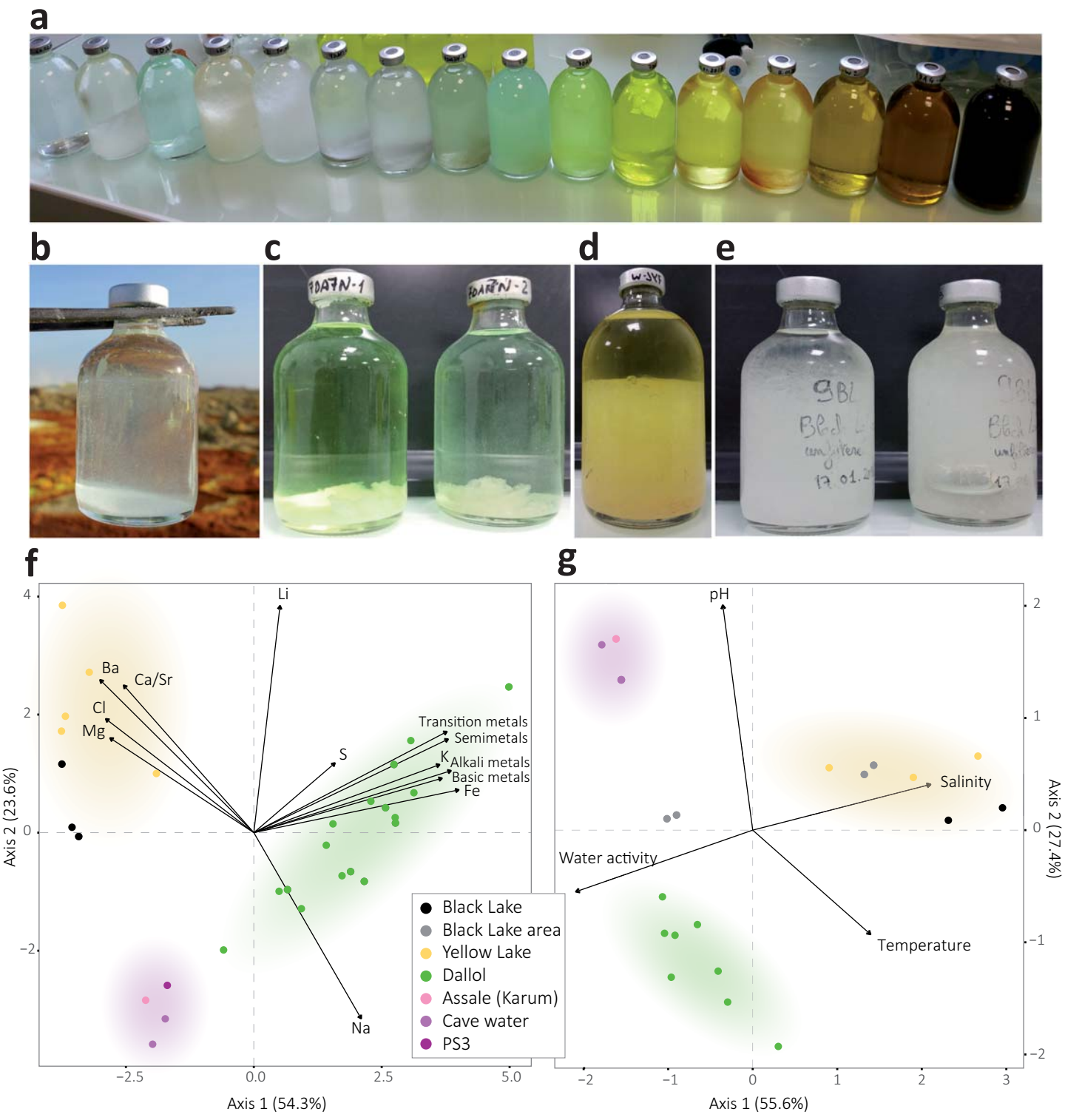

Figure 2. Belilla et al.

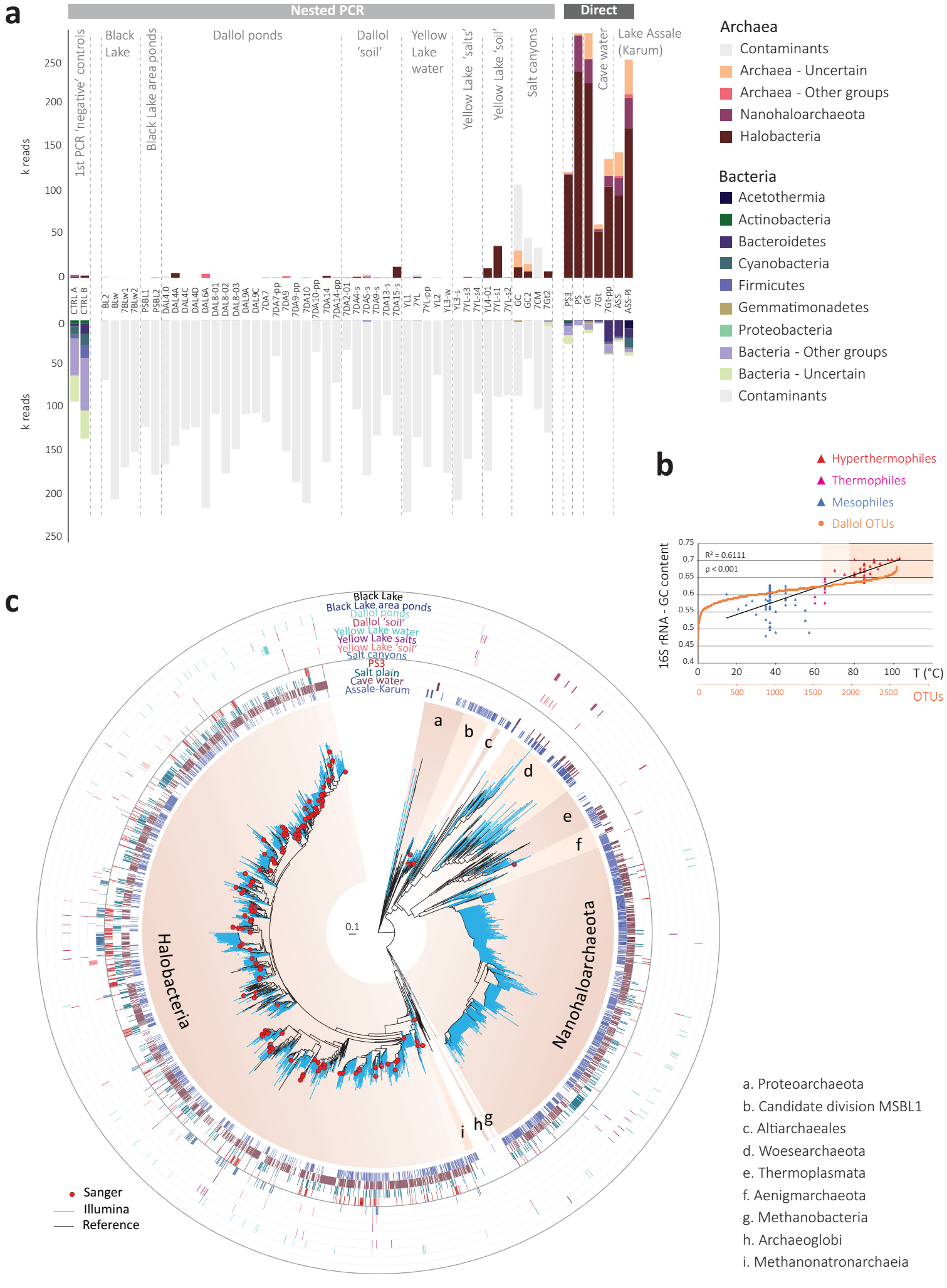

a. Proteoarchaeota
b. Candidate division MSBL1
c. Altiarchaeales
d. Woesearchaeota
e. Thermoplasmata
f. Aenigmarchaeota
g. Methanobacteria
h. Archaeoglobi
i. Methanonatronarchaeia

Figure 3. Belilla et al.

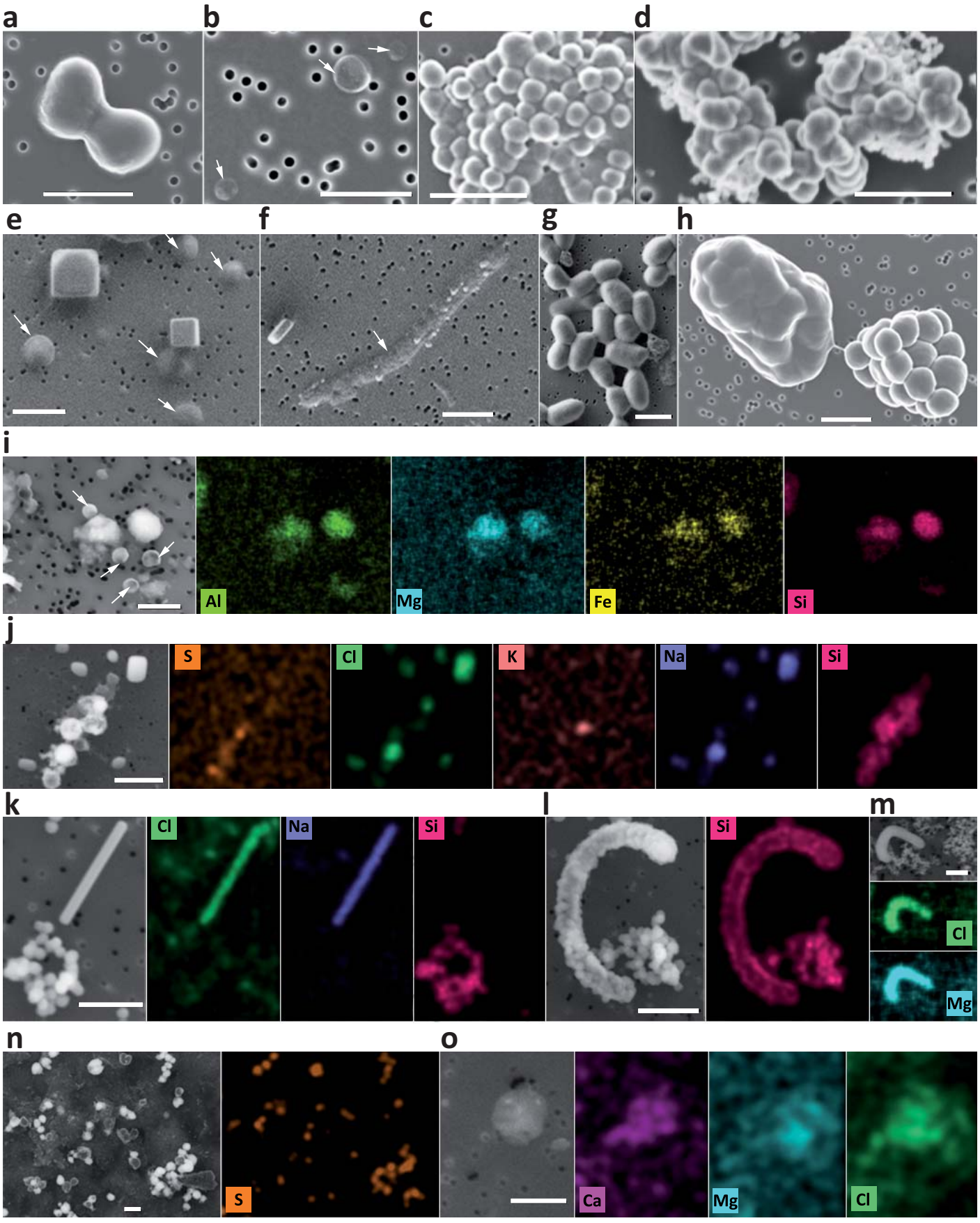

Figure 4. Belilla et al.

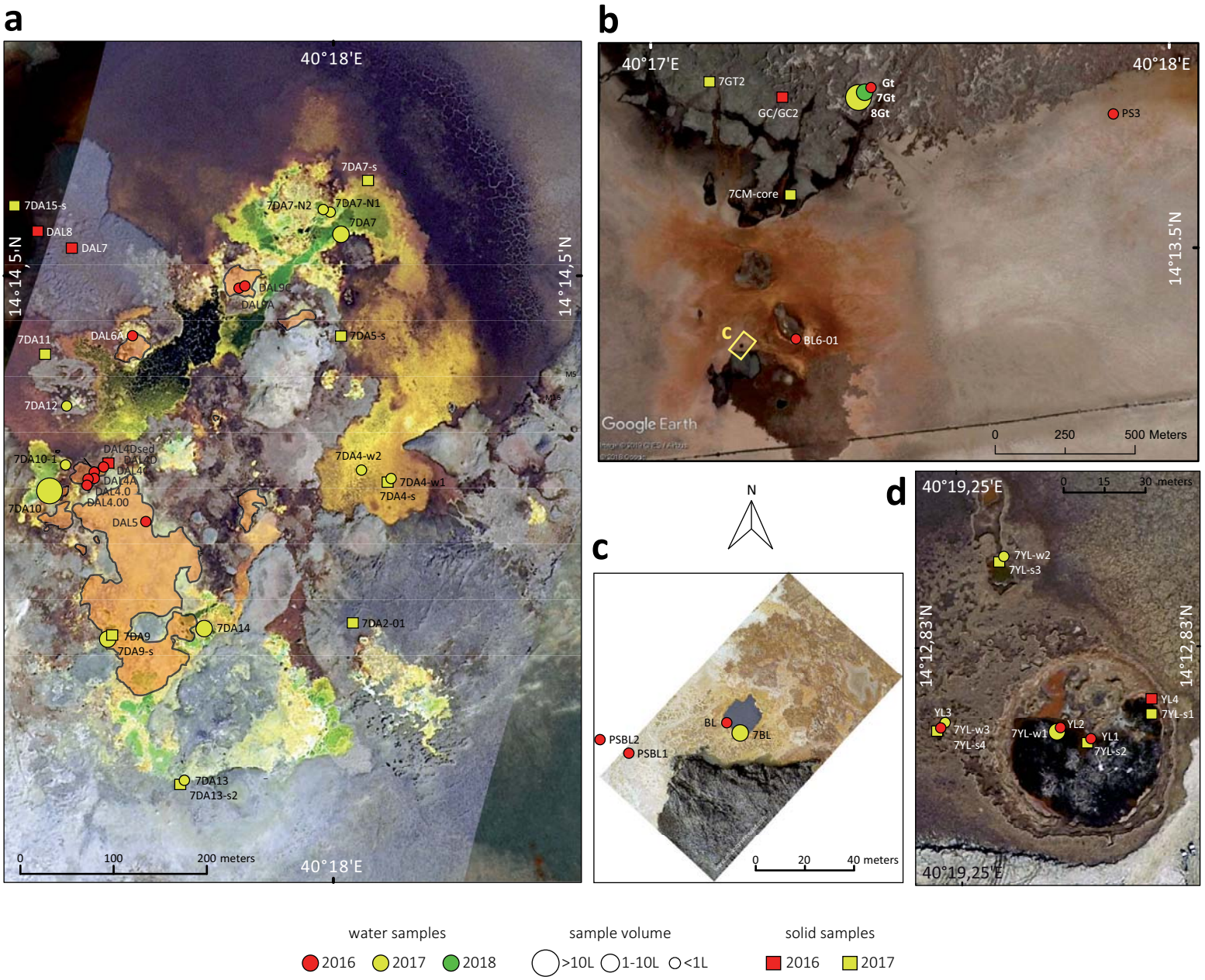

Extended Data Fig. 1 | Aerial view of the main sampling sites in the Dallol area. a, Dallol dome summit showing the acidic green-yellow-brown colored hydrothermal ponds and active degassing areas during our 2017 sampling trip; the orange-shaded area shows the active hydrothermal zone in January 2016. **b**, Dallol West salt canyons and Black Mountain area. **c**, Black Lake. **d**, Yellow Lake and surroundings. Names of samples and sampling sites are indicated. The size of circles is proportional to the water volume collected or filtered for subsequent analyses. Aerial photographs were taken from a drone by O. Grunewald, except b, which is a Google Earth aerial image (09/03/2016) provided by Image © 2019 CNES/Airbus.

Extended Data Fig. 2 | Views of different sampling sites in the Dallol dome and surroundings in the Danakil Depression. a, DAL4 sampling site ponds; **b**, DAL5 pond and active degassing area; **c**, active hydrothermal springs in DAL9 ponds; **d**, in situ cell-trap filtration at the 7DA7 sampling area; **e**, 7DA9 sampling site; **f**,7DA10 ponds showing increasingly darker and brownish colors along the oxidation gradient; **g**, water samples from the different 7DA10 ponds; **h**, DAL8 mineral precipitates; **i**, 'proto-soil'-like salt crust (7YL-S1) near the Yellow Lake; **j**, Yellow Lake showing active degassing; **k**, YL3, salt-mud volcano in the Yellow Lake area; **l**, 'Little Dallol' hydrothermal very active area in 2016 on the way to the Black Mountain (in the distance; inlet, chimney emitting hydrocarbon-rich fluids at 110°C); **m**, Black Lake; **n**, PSBL2 (Black Lake area ponds); **o**, wet salt plain, influenced by hydrothermal activity, corresponding to PS3 sample area; **p**, the cave in the salt canyons where Gt, 7Gt and 8Gt samples were collected; **q**, salt canyons; **r**, Assale (Karum) lake. Sample names starting by 7 indicate collection in 2017. Pictures from all other samples/sampling sites were taken during the 2016 expedition.

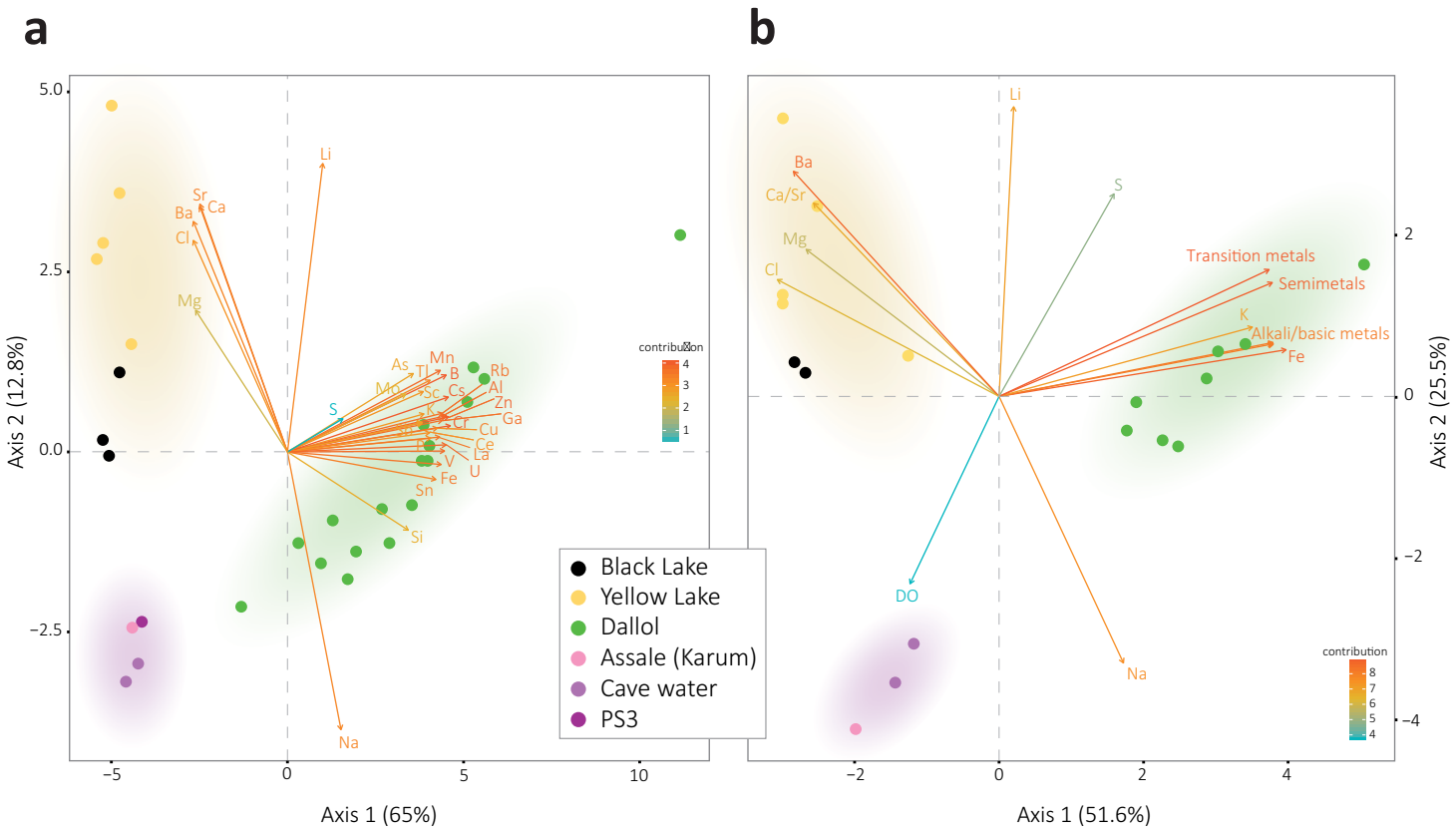

Extended Data Fig. 3 | Principal Component Analyses (PCA) of Dallol area sampling sites as a function of physicochemical parameters. a, PCA of 29 samples according to their chemical composition; only relatively abundant elements (see Supplementary Table 1) are included in the analysis. A summary of this analysis is shown in Fig.2f. **b**, PCA including the same variables as Fig. 2f but additionally including dissolved oxygen (DO). Measured parameters on site can be found in Extended Data Table 1. Colored zones in PCA analyses correspond to the three major chemical zones identified in this study.

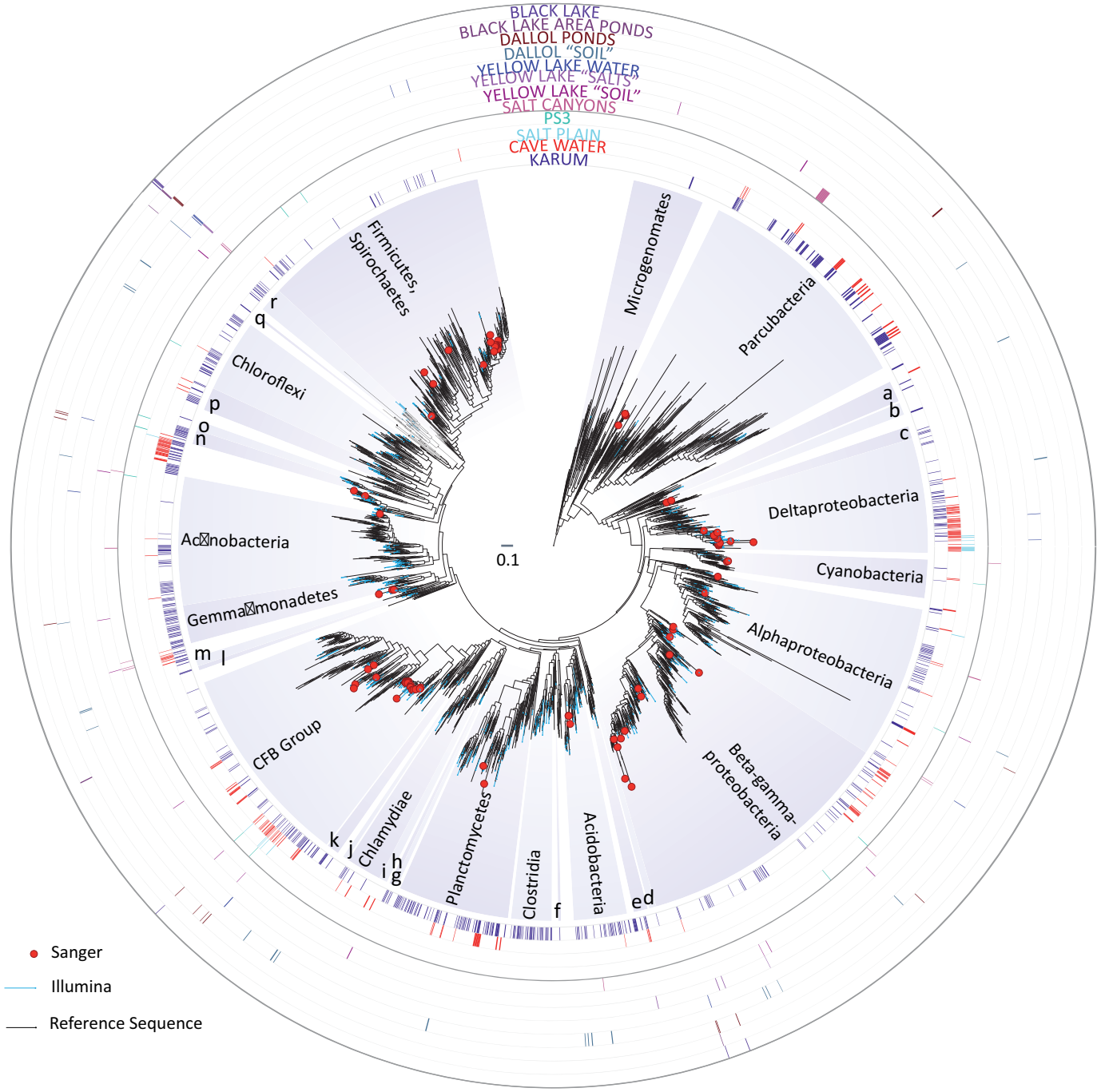

a. Peregrinibacteria
b. Saccharibacteria
c. Desulfovibrionales
d. Deferribacteres
e. Candidate division TM6
f. Candidate division NC10
g. Candidatus Latescibacteria
h. Candidatus BRC1
i. Omnitrophica
j. Zixibacteria
k. Marinimicrobia
l. Rokubacteria
m. Nitrospirae
n. Acetothermia
o. Synergistetes
p. Armatimonadetes
q. Dadabacteria
r. Deinococcus-Thermus

Extended Data Fig. 4 | Phylogenetic tree of bacterial 16S rRNA gene sequences showing the phylogenetic placement of OTUs identified in the different Dallol area samples. Sequences derived from metabarcoding studies are represented by blue lines (Illumina sequences); those derived from cloning and Sanger sequencing of environmental samples, cultures and FACS-sorted cells are labelled with a red dot. Reference sequences are in black. Concentric circles around the tree indicate the presence/absence of the corresponding OTUs in different groups of samples (groups shown in Fig.3a). Only sequences not deemed contaminant (see Supplementary Table 5) were included in the tree. The full tree is provided as Supplementary Data 2.

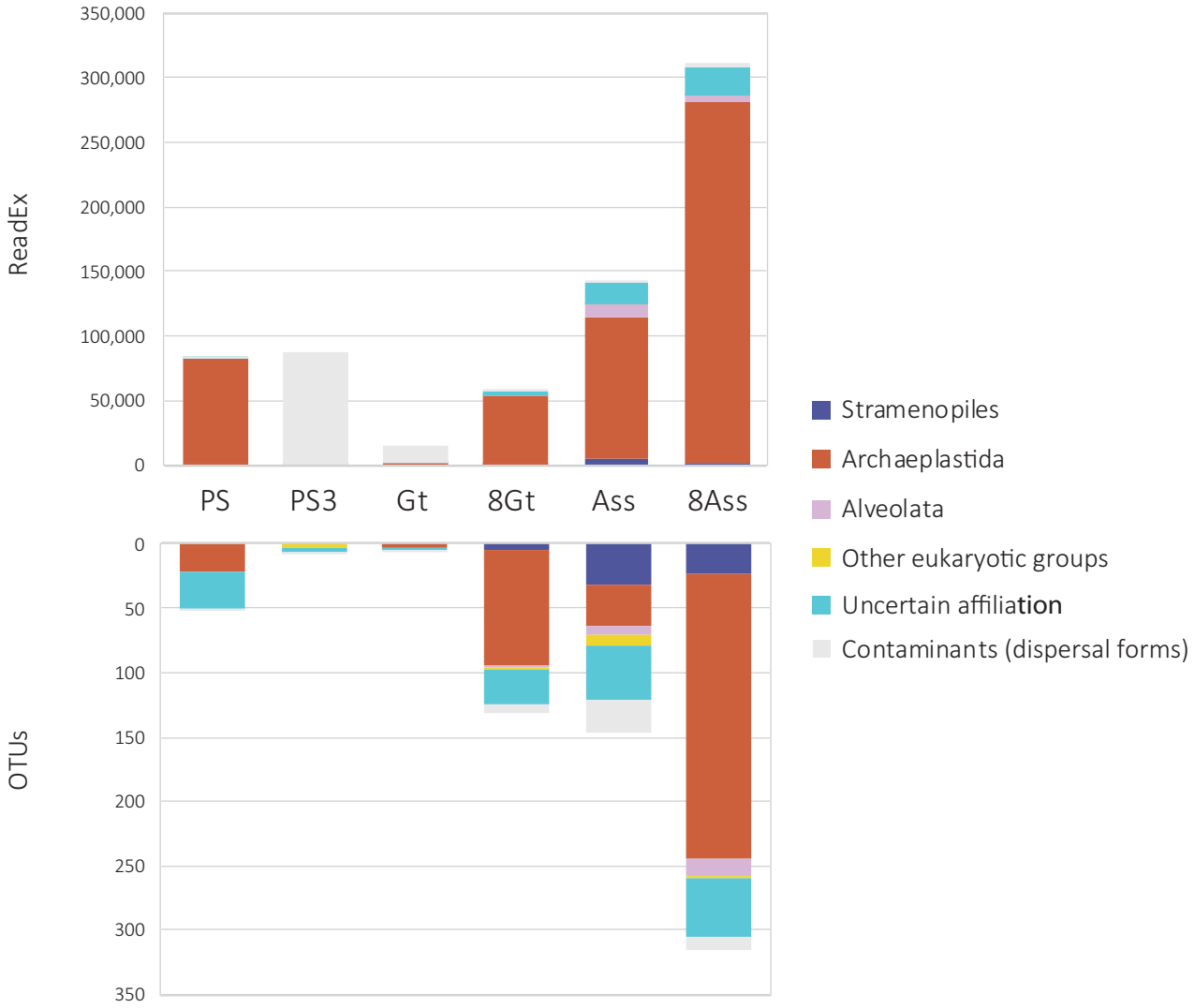

Extended Data Fig. 5 | Eukaryotic presence, diversity and relative abundance in Dallol area samples. Histogram showing the phylogenetic affiliation and abundance of 18S rRNA gene amplicon reads of eukaryotes (upper panel) obtained with universal eukaryotic primers and the associated OTU diversity (lower panel). Only a few samples yielded amplicons; negative PCR controls were always negative. Sequences corresponding to macroscopic plants and fungi (probably derived from pollen or spores) were considered contaminant (light grey). The phylogenetic affiliation of dominant eukaryotic groups is color-coded.

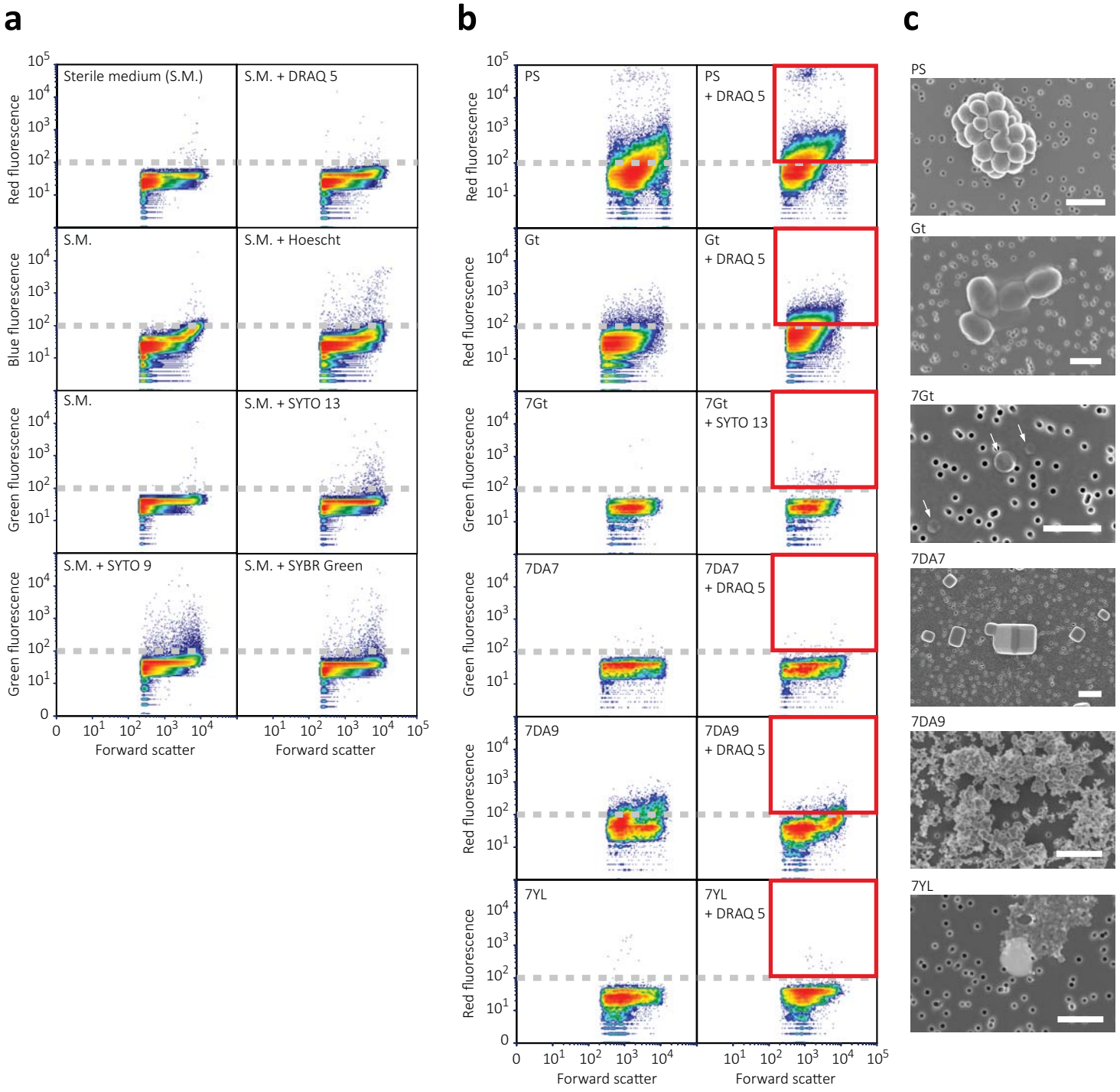

Extended Data Fig. 6 | Multiparametric fluorescence analyses and fluorescence-activated cell sorting (FACS) analyses of representative Dallol area samples. a, effect of DNA fluorescent dyes on background fluorescence emission; natural (left panels) and DNA dye-induced (right panels) fluorescence in the sterile hypersaline SALT-YE medium used to dilute/sort Dallol samples. Fluorescence is plotted against the size of the analyzed particles (forward scatter); events concentration is color-coded, red being high concentration and blue, low concentration. DRAQ 5 and SYTO 13 introduced less background and were chosen for FACS of natural samples. The approximate background threshold (ca. 10^2) is indicated by a broken grey line. **b**, multiparametric fluorescence analyses of different Dallol samples before (left panels) and after (right panels) adding fluorescent DNA dyes. Events (particles) above background (red squares) were FACS-sorted and filtered on 0.1 µm pore-size filters prior to SEM observations. **c**, SEM photographs showing examples of sorted particles. Cells are observed in samples PS, Gt and 7Gt; halite crystals in 7DA7 and amorphous mineral particles in 7DA9 and 7YL. Arrows indicate ultrasmall cells. The scale bar is 1 µm.

Extended Data Table 1 | List and description of samples from the Dallol area analyzed in this study and type of analyses performed. DO, dissolved oxygen; ORP, oxido-reduction potential; SEM/EDXS, scanning electron microscopy/energy-dispersive x-ray spectrometry; FACS, fluorescence-activated cell sorting analysis; n.a., not applicable; n.d. not determined. Refractometry-derived salinity refers to the percentage (w/v) of local salt composition (see Supplementary Tables 1 and 3 for elementary and ionic analyses) measured in situ. Salinity was also directly measured by weighting the total solids (dry weight experimentally measured in triplicates; SD, standard deviation).

Color of ponds or solid samples	Sample name	Coordinates	Collection date	Brief description	Sample type / volume			Physicochemical parameters						Type of analyses					
					Solid	Liquid (ml)	0.2-30 µm fraction (ml)[a]	Temp (°C)	pH	DO (%)	DO (mg/l)	ORP (mV)	Refractometry inferred salinity (%)	Salinity - Total Solids (g/l) ± SD	Chemistry	Cloning/ Sanger seq.	Meta-barcoding	Culture assays[b]	SEM/ EDXS	FACS
Dallol hydrothermal ponds																			
	DAL4.00	14.23916N 40.297059E	16.01.2016	Hydrothermal fluid from a salt chimney feeding cascading ponds along redox gradient site DAL4		50	1000	108.0	n.d	n.d	n.d	n.d	30.0	375.40 ± 10.06	X	X				
	DAL4.0	14.23923N 040.29707E	17.01.2016	Warm whitish green pond in the redox pond series DAL4		50	1000	46.3	-0.43	0.55	0.03	328.95	21.0	373.29 ± 4.83	X	X	X	Y	X	
	DAL4A	14.23921N 040.29713E	17.01.2016	Bright green pond in the redox pond series DAL4		50	1000	30.5	-0.53	3.05	0.26	366.8	22.0	n.d	X	X	X	Y	X	
	DAL4C	14.23967N 040.29744E	16.01.2016	Brownish green pond in the redox pond series DAL4			1000	31.6	-0.95	1	0.08	384.05	21.5	n.d		X	X	Y		
	DAL4D	14.23934N 040.29728E	16.01.2016	Dark brown pond along an oxidation gradient, DAL4 site		50	1000	31.0	-0.72	1.4	0.11	381.55	n.d	405.32 ± 19.6	X	X	X	Y	X	
	DAL 4D-SED	14.23934N 040.29728E	16.01.2016	Yellow salt front forming pond wall	X			n.a	n.a	n.a	n.a	n.a	n.a	n.a	X	X				
	DAL 5	14.23869N 40.29776E	17.01.2016	Yellow water from one big Dallol pond		50		42.6	-0.93	3.4	0.19	373.3	40	386.84 ± 6.18				Y		
	DAL6A	14.24083N 040.29756E	18.01.2016	Fluid from a salt chimney feeding various ponds along an oxidation gradient, site DAL6		50	1000	108.4	-0.65	n.d	n.d	n.d	n.d	424.51 ± 38.22	X	X	X	Y		
	DAL 7	14.242343N 40.296798E	18.01.2016	Sulfur-colored mineral precipitates on "chocolate formation"	X			n.a	n.a	n.a	n.a	n.a	n.a	n.a				Y		
	DAL8-01	14.24217N 040.29635E	20.01.2016	Yellow, potentially sulfur-rich precipitates	X			n.a	n.a	n.a	n.a	n.a	n.a	n.a		X	X	Y		
	DAL8-02	14.24217N 040.29635E	20.01.2016	Golden, potentially sulfur-rich salt precipitates	X			n.a	n.a	n.a	n.a	n.a	n.a	n.a		X	X			
	DAL8-03	14.24217N 040.29635E	20.01.2016	Brown, potentially sulfur-rich salt precipitates	X			n.a	n.a	n.a	n.a	n.a	n.a	n.a		X	X			
	DAL9A	14.241504N 40.298836E	21.01.2016	Large ligth green bubbling pond with various hydrothermal sources; site DAL9		50	650	37.9	-0.27	n.d	n.d	n.d	n.d	n.d	X	X	X	Y		
	DAL9C	14.24151N 40.298874E	21.01.2016	Smaller deep green hydrothermal pond at the DAL9 site		50	750	56.0	-0.20	n.d	n.d	n.d	n.d	n.d	X	X	X			
	7DA2-01	14.241275N 40.300633E	06.01.2017	Grey cauliflower-like mineral precipitates	X			n.a	n.a	n.a	n.a	n.a	n.a	n.a		X	X			
	7DA4-w1	14,239406N 40,300419E	10.01.2017	Yellow-brownish water from a drying pond formed by yellow-colored salt		100		27.9	-0.73	3.8	0.13	416.1	44	446.07 ± 11.41	X					
	7DA4-w2	14,239892N 40,300106E	10.01.2017	Slightly lighter water from the same kind of pool as 7DA4-w1		100		27.0	-0.72	2.9	0.09	420.1	40	371.77 ± 2.11	X					
	7DA4-s	14,239406N 40,300419E	10.01.2017	Fresh, yellow cauliflower-like mineral precipitates near 7DA4-w2	X			n.a	n.a	n.a	n.a	n.a	n.a	n.a		X	X			
	7DA5-s	14,240908N 40,300119E	10.01.2017	Brown (oxidized), fluid-impregnated cauliflower-like mineral precipitates	X			n.a	n.a	n.a	n.a	n.a	n.a	n.a	X	X	X			
	7DA7	14.24219N 40.300102E	07.01.2017	Water from an active green large pond fed by multiple hydrothermal springs		500	3000	19.7	-0.55	4.1	0.16	371.9	47	429.6 ± 12.89		X	X	X	X	X
	7DA7-s	14.2428N 40.300494E	10.01.2017	Brown salt crust East to 7DA7 active site on a drying pondcovering a layer of wet yellow salt	X			n.a	n.a	n.a	n.a	n.a	n.a	n.a	X					
	7DA7N-1	14.242381N 40.299992E	10.01.2017	Bluish hot pond on the northern terrace feeding 7DA7		50		44.6	-0.33	5.7	0.16	271.2	40.0	404.13 ± 20.16	X			Y		
	7DA7N-2	14.242381N 40.299992E	10.01.2017	Hotter, greenish pond adjacent to 7DA7N-1		50		68.0	n.d	n.d	n.d	n.d	37.0	411.1 ± 0.57	X					
	7DA9	14.241528N 40.29884E	08.01.2017	Large pond in active degassing area with many white-yellowish chimneys and salt nenuphars		500	6000	31.9	-0.34	5.5	0.16	369	43	379.03 ± 17.18	X	X	X	X	X	X
	7DA9-s	14.241528N 40.29884E	08.01.2017	Centimetric round-shaped salt and sulfur formations in a dry pond next to 7DA9	X			n.a	n.a	n.a	n.a	n.a	n.a	n.a		X	X			
	7DA10	14.23908N 40.296598E	09.01.2017	Upper green pond in a well-marked terrace system along an oxidation gradient		100	14700	55.2	-0.08	2.2	0.05	321.8	35.0	366.83 ± 7.71	X	X	X			
	7DA10-1	14.23908N 40.296598E	09.01.2017	Highly evaporated, dark brown pond, lower in the 7DA10 terrace system		100		33.4	n.d	n.d	n.d	n.d	70	n.d	X			Y		
	7DA12	14.240136N 40.29675E	10.01.2017	Active chimney (nearby 2016 site DAL6)		100		108.3	0.47	n.d	n.d	n.d	43.0	385.48 ± 21.18	X					
	7DA13-w1	14.235495N 40.298135E	11.01.2017	Hydrothermal fluid from big grey active chimney		100		103.6	n.d	n.d	n.d	n.d	35.0	342.50 ± 18.87	X					
	7DA13-s2	14.235495N 40.298135E	11.01.2017	Grey, hard salt fragments at the bottom of chimney 7DA13	X			n.a	n.a	n.a	n.a	n.a	n.a	n.a		X	X			
	7DA14	14.237398N 40.298428E	12.01.2017	Central pond in active group of geothermal ponds. Green color		50	675	39.7	-0.51	2.4	0.15	382	40	338.90 ± 8.17	X	X	X			
	7DA15-s	14.2421427N 40.297727E	13.01.2017	Green/yellow sediment near the "chocolate formation" CH-F	X			n.a	n.a	n.a	n.a	n.a	n.a	n.a		X	X			
Yellow Lake (Gaet'Ale)																			
	YL1	14.213574N 40.32128E	19.01.2016	Yellow Lake bubbling water, yellow-orange color, oily textyre, smell of organics-containing gas	X	50	400	40.6	1.88	6.6	0.37	447.1	>50	724.40 ± 5.77	X	X	X	Y	X	
	YL2	14.213648N 40.321188E	19.01.2016	Yellow Lake bubbling water - nearby spot (few meters away)		50	400	39.5	1.88	5.4	0.35	419.3	51.0	677.60 ± 2.24	X	X	X	Y		
	YL3-01-w	14.213598N 40.320748E	19.01.2016	Water from salt/sediment volcano			400	37.1	n.d	n.d	n.d	n.d	>50	761.59 ± 69.51		X	X	Y	X	
	YL3-01-s	14.213598N 40.320748E	19.01.2016	Salty deposits from bubbling salt/sediment volcano - reddish color	X			37.1	n.a	n.a	n.a	n.a	n.a	n.a		X	X			
	YL4-01	14.21386N 40.321482E	19.01.2016	Salt crust on top of sediment at the further upper rim of Yellow Lake	X			n.a	n.a	n.a	n.a	n.a	n.a	n.a		X	X			
	7YL-w1	14.213574N 40.32128E	12.01.2017	Water from the Yellow Lake		150	5000	37.4	1.52	11.5	0.63	462.2	>50	944.60 ± 60.38	X			X	X	
	7YL-w2	14.213648N 40.321188E	12.01.2017	Water from a mid-sized pond near the Yellow Lake, strong smell of organics, dead birds		200		33.8	2.40	4.4	0.20	310.3	70	683.80 ± 80.61	X			X		X
	7YL-w3	14.213598N 40.320748E	12.01.2017	Water from salt mud volcano (YL3 in 2016)		100		35.9	1.37	5.1	0.32	349.3	80	n.d	X			X		
	7YL-s1	14.213574N 40.32128E	12.01.2017	Salt crust from dried area in Yellow Lake	X			n.a	n.a	n.a	n.a	n.a	n.a	n.a		X	X			
	7YL-s2	14.213648N 40.321188E	12.01.2017	Pinkish salt forming ripple marks on the rim of the Yellow Lake	X			n.a	n.a	n.a	n.a	n.a	n.a	n.a		X	X			
	7YL-s3	14.213598N 40.320748E	12.01.2017	Salt fragments from rim of 7YL-w2	X			n.a	n.a	n.a	n.a	n.a	n.a	n.a	X	X	X			
	7YL-s4	14.2136083N 40.3212611E	12.01.2017	Reddish salt/sediment from salt mud volcano	X			n.a	n.a	n.a	n.a	n.a	n.a	n.a		X	X			
Black Lake and surroundings																			
	PSBL1	14.221732N 40.28582E	19.01.2016	Reddish salt and water from pond close to Black Lake		50		40.6	2.63	n.a	n.a	n.a	62.0	643.40 ± 22.20		X	X	XY		
	PSBL2	14.221788N 40.285713E	19.01.2016	Yellowish salt and water from pond close to Black Lake		50		40.6	2.50	n.a	n.a	n.a	58.0	620.4		X	X	XY		
	PSBL3	14.22173N 040.28582E	19.01.2016	Orange salt and water from pond between Black Lake and camp site		50		n.d	n.d.	n.a	n.a	n.a	34.0	344.40 ± 10.77				XY	X	
	PSBL4	14.22173N 040.28582E	22.01.2016	Warm red pond with acid emissions		50		40.0	3.50	n.a	n.a	n.a	38.0	366.67 ± 9.63				X	X	
	BL2	14.221842N 40.286173 E	19.01.2016	Black Lake bischofite-enriched water, very high viscosity		25		n.a	n.a	n.a	n.a	n.a	n.a	n.d		X				
	BL / BL1-02 / BL-w	14.22182N 40.286208E	19.01.2016	Black Lake bischofite-enriched water, very high viscosity		50	150	70.6	3.50	n.a	n.a	n.a	n.a	819.83 ± 181.88	X	X	X	Y		
	BL6-01	14.22211N 40.28805E	24.01.2016	Black fluid from chimney in very active young geothermal formation, black dome area		15		110.0	4.40				n.d	n.d				Y		
	7BL-w1	14.22182N 40.286208E	10.01.2017	Black Lake bischofite-enriched water from surface		150		60.1	2.57	2.8	0.11	226.9	76	718.94 ± 17.94	X		X	X		
	7BL-w2	14.22182N 40.286208E	10.01.2017	Black Lake bischofite-enriched water, 3 m depth		100		n.a	n.a	n.a	n.a	n.a	n.a	n.d	X		X	Y		
Salt plain at Dallol dome base																			
	PS	14.2250194N 40.2889000E	19.01.2016	Salt pan fragment between the Dallol dome and Black Lake, rehydrated with sterile spring water	X	100	30	n.a	n.a	n.a	n.a	n.a	n.a	n.a		X	X	X	X	X
	PS3	14.22912N 40.297935E	19.01.2016	Water from salt shallow, hydrothermally influenced, pond at the dome base		150	950	29.3	4.21	n.d	n.d	n.d	20.0	352.64 ± 10.78	X	X	X	XY	X	
Lake Assale (Lake Karum)																			
	Ass	14.089567N 40.348583E	23.01.2016	Water from Lake Assale (Karum), overflooded towards the North of the Danakil Depression			8000	26.2	6.68	53.0	4.30	97.7	20.0	360.72 ± 11.52		X	X	X		
	8Ass	14.089567N 40.348583E	15.01.2018	Water from Lake Assale (Lake Karum)		100	3000	22.0	6.54	14	2.82	221	31	363.15 ± 11.51	X	X		XY	X	
Dallol Salt Canyons																			
	Gt	14.229704N 40.289952E	18.01.2016	Cave hypersaline water reservoir at the salt canyons, West Dallol dome		50	50	n.d	n.d	n.d	n.d	n.d	30	n.d		X	X	XY	X	X
	7Gt	14.229704N 40.289952E	11.01.2017	Cave hypersaline water reservoir at the salt canyons, West Dallol dome		100	10000	29.0	6.27	9.5	0.27	117.2	30	323.87 ± 19.39		X	X	XY	X	X
	7Gt2	14.23043N 40.285295E	13.01.2017	Small core at the mouth of a dry subterranean stream bed at the Western Dallol salt canyons	X			n.a	n.a	n.a	n.a	n.a	n.a	n.d		X	X			
	8Gt	14.23043N 40.285295E	16.01.2018	Cave hypersaline water reservoir at the salt canyons, West Dallol dome		100	3000	22.0	6.54	15.2	2.30	262.1	30	330.82 ± 10.78	X	X		X	X	
	GC/GC2	14.229658N 40.287723E	15.01.2016	Gypsum crust from Dallol West salt canyons	X			n.a	n.a	n.a	n.a	n.a	n.a	n.a	X	X	X			
	7CM-core	14.226668N 40.287813E	13.01.2017	Small core of hydrothermally-influenced orange salty mud core at the base od the dome	X			n.a	n.a	n.a	n.a	n.a	n.a	n.a		X	X			

[a] Volume of water filtered to retain particles/cells in the indicated size range

[b] Samples labeled X and Y represent independent culture assays in two different laboratories (X-Orsay, Y-Madrid)

Extended Data Table 2 | Chaotropicity, ionic strength and water activity for a selection of samples of the Dallol area.
Chaotropicity was measured experimentally (see Methods) and also calculated, together with ionic strength values were from dominant Na, K, Mg, Ca, Fe chemistry data; water activity values were measured using a probe (see Methods). Known limits for life for each parameter are listed at the top of the table. Samples beyond that threshold for one or more of those parameters are shaded in grey.

		Measured chaotropicity (kJ/kg)	Calculated chaotropicity (kJ/kg)	Ionic strength (mol/L)	Water activity (a_w)
Life threshold*		**≤87.3**		**≤12.141**	**≥0.585**
Cave water	Gt		n.d	n.d	0.728
	7Gt	-18.3	-23.80	4.751	0.729
	8Gt	-57.5	-56.65	6.873	0.731
Lake Assale	8Ass	n.d.	7.10	7.274	0.718
Geothermally influenced Salt Plain	PS3	n.d.	24.09	7.138	n.d
Dallol dome hydrothermal pools	DAL 4.00	-21.7	-17.87	6.104	0.719
	DAL 4.0	n.d.	-18.71	7.307	n.d
	DAL 4A	n.d.	-9.61	6.346	n.d
	DAL 4D	n.d.	2.14	7.104	n.d
	DAL 6A	n.d.	-23.97	7.203	n.d
	DAL 9A	n.d.	-7.77	7.529	n.d
	DAL 9C	n.d.	-16.15	8.349	n.d
	7DAL4-W1	19.3	40.44	6.314	0.667
	7DAL4-W2	8.3	14.28	5.383	0.698
	7DAL7	8.8	19.64	5.989	0.694
	7DAL-N1	9.2	20.84	6.472	0.694
	7DAL-N2	11.5	11.01	5.940	0.698
	7DAL9	-8.2	2.95	5.176	0.708
	7DAL10	2.1	-7.46	5.037	0.714
	7DAL10-1	n.d	n.d	n.d	**0.580**
	7DAL12	-31.2	-20.57	5.793	n.d
	7DAL13-W1	-24.8	-20.13	4.785	0.723
	7DAL14	-11.7	7.54	5.307	0.748
Black Lake area pools	PSBL1	**108.3**	n.d	n.d	**0.334**
	PSBL2	**93.5**	n.d	n.d	**0.345**
	PSBL3	63.4	n.d	n.d	0.722
	PSBL4	61.8	n.d	n.d	0.711
Black Lake	BL	**288.3**	**354.19**	**19.155**	**0.319**
	7BL-W1	**198.5**	**259.41**	**14.206**	**0.322**
	7BL-W2	**201.3**	**268.89**	**14.721**	n.d
Yellow Lake	YL1	n.d.	**492.06**	**19.141**	n.d
	YL2	n.d	**574.04**	**22.085**	n.d
	YL3	**231.8**	n.d	n.d	**0.319**
	7YL-W1	**320.8**	**495.01**	**18.446**	**0.261**
	7YL-W2	**308.2**	**328.92**	**13.796**	**0.467**
	7YL-W3	n.d.	**466.64**	**17.609**	n.d

* Data from Hallsworth et al (2007) and Stevenson et al (2015 and 2017)

Extended Data Table 3 | Sequence data and diversity measurements. *Contaminant sequences included sequences identified in negative controls and/or high similarity to human-associated bacteria; s.e., standard error. Eventual mitochondrial and chloroplast 16S rRNA gene sequences were also removed at this step.

Sample name	Initial No. of merged reads	No. of high quality reads	No. of retained reads after chimera check	No. of retained reads after removing contaminants*	No. archaeal reads	No. OTUs	Diversity (Simpson index)	Evenness	Richness (Chao1) (s.e.)	No. of bacterial reads	No. OTUs	Diversity (Simpson index)	Evenness	Richness (Chao1) (s.e.)
Prokaryotic sequences							**Archaea**					**Bacteria**		
DAL4.0	169949	169648	165257	4	3	2	0.44	0.92	2 (0)	1	1	0.00	NA	1 (0)
DAL4A	152469	152298	146065	5023	5023	2	0.00	0.01	2 (0)	0	0	1.00	0.00	0 (NA)
DAL4C	126853	126665	123020	0	0	0	1.00	0.00	0 (NA)	0	0	1.00	0.00	0 (NA)
DAL4D	125034	124804	120619	0	0	0	1.00	0.00	0 (NA)	0	0	1.00	0.00	0 (NA)
DAL6A	234168	233935	224050	4314	4303	21	0.03	0.03	35 (11)	11	4	0.45	0.64	7 (4)
DAL8-01	113894	112383	108675	6	0	0	1.00	0.00	0 (NA)	6	2	0.28	0.65	2 (0)
DAL8-02	182460	176331	172030	2	0	0	1.00	0.00	0 (NA)	2	2	0.50	1.00	3 (2)
DAL8-03	154815	151700	148869	41	0	0	1.00	0.00	0 (NA)	41	4	0.34	0.49	4 (0)
DAL9A	132758	131862	126420	2	0	0	1.00	0.00	0 (NA)	2	2	0.50	1.00	3 (2)
DAL9C	107108	106589	104746	0	0	0	1.00	0.00	0 (NA)	0	0	1.00	0.00	0 (NA)
7DA7	133151	132970	128002	1	1	1	0.00	NA	1 (0)	0	0	1.00	0.00	0 (NA)
7DA7-pp	42089	42043	41253	2	2	2	0.50	1.00	3 (2)	0	0	1.00	0.00	0 (NA)
7DA9	158516	158249	152576	1821	1	1	0.00	NA	1 (0)	0	0	1.00	0.00	0 (NA)
7DA9-pp	217467	217096	192709	2	0	0	1.00	0.00	0 (NA)	2	1	0.00	NA	1 (0)
7DA10	213263	212784	205528	1	1	1	0.00	NA	1 (0)	0	0	1.00	0.00	0 (NA)
7DA10-pp	44566	44540	40224	62	0	0	1.00	0.00	0 (NA)	62	2	0.03	0.12	2 (0)
7DA14	168809	168500	162187	2096	2094	5	0.01	0.02	5 (0)	2	2	0.50	1.00	3 (2)
7DA14-pp	82248	82170	71068	471	345	30	0.94	0.89	32 (3)	126	7	0.69	0.72	7 (0)
7DA2-01	33880	33832	33711	45	31	5	0.68	0.82	5 (0)	14	7	0.83	0.94	9 (3)
7DA4-s	103418	103261	102476	1492	1490	13	0.81	0.69	15 (3)	2	2	0.50	1.00	3 (2)
7DA5-s	184910	184641	180701	5243	3208	22	0.91	0.82	32 (10)	2035	19	0.84	0.78	19 (0)
7DA9-s	130399	130259	129730	261	212	8	0.72	0.70	9 (1)	49	1	0.00	NA	1 (0)
7DA13-s	100425	100280	99550	298	298	7	0.66	0.67	7 (0)	0	0	1.00	0.00	0 (NA)
7DA15-s	143741	143552	142694	12589	12460	11	0.06	0.08	11 (0)	129	2	0.48	0.97	2 (0)
YL1	226774	226389	217444	42	1	1	0.00	NA	1 (0)	41	4	0.30	0.43	5 (2)
7YL	178284	177903	172455	1770	1302	13	0.57	0.47	13 (0)	468	7	0.74	0.76	7 (0)
7YL-pp	65597	65556	62547	0	0	0	1.00	0.00	0 (NA)	0	0	1.00	0.00	0 (NA)
YL2	153107	152918	144028	2	2	1	0.00	NA	1 (0)	0	0	1.00	0.00	0 (NA)
YL3-01w	188511	188312	172260	126	0	0	1.00	0.00	0 (NA)	126	3	0.03	0.08	4 (2)
YL3-01s	232822	232611	210691	3	0	0	1.00	0.00	0 (NA)	3	2	0.44	0.92	2 (0)
7YL-s3	158645	158488	157145	979	898	15	0.86	0.83	15 (0)	81	4	0.07	0.14	7 (4)
7YL-s4	86468	86366	85180	207	157	4	0.60	0.76	4 (0)	50	2	0.08	0.24	2 (0)
YL4.01	200889	200588	191536	10711	10691	2	0.00	0.00	2 (0)	20	3	0.27	0.47	3 (0)
7YL-s1	124032	123877	122505	36177	36016	39	0.79	0.50	39 (0)	161	6	0.79	0.91	6 (0)
7YL-s2	85188	85072	84444	668	547	10	0.75	0.70	10 (0)	121	5	0.71	0.83	5 (0)
BL2	76395	76209	73977	12	0	0	1.00	0.00	0 (NA)	12	6	0.78	0.91	8 (3)
BLw	227966	227636	218708	0	0	0	1.00	0.00	0 (NA)	0	0	1.00	0.00	0 (NA)
7BLw1	177297	177131	171404	3	0	0	1.00	0.00	0 (NA)	3	1	0.00	NA	1 (0)
7Blw2	158986	158630	151304	1	0	0	1.00	0.00	0 (NA)	1	1	0.00	NA	1 (0)
PSBL1	127518	127100	124137	8	0	0	1.00	0.00	0 (NA)	8	4	0.66	0.88	5 (1)
PSBL2	181312	180562	177286	5	3	2	0.44	0.92	2 (0)	2	1	0.00	NA	1 (0)
PS3	150482	149968	146028	146028	118980	291	0.88	0.56	313 (7)	26537	123	0.96	0.56	138 (11)
PS	304190	303656	282495	282495	274013	602	0.94	0.51	701 (22)	5893	39	0.30	0.51	50 (8)
ASS	173226	172959	165299	165299	140633	1013	0.94	0.59	1190 (33)	23963	496	0.69	0.59	544 (13)
ASS-PJ	314682	314213	288299	288299	244551	1349	0.94	0.57	1441 (18)	39873	859	0.88	0.57	912 (12)
GT	303592	303083	288086	288086	274039	656	0.87	0.53	755 (25)	14047	173	0.91	0.53	193 (11)
7GT	71483	71368	64143	64143	59788	524	0.95	0.57	735 (46)	4353	147	0.92	0.57	201 (22)
7Gt-pp	235497	235111	172010	172010	132967	1495	0.97	0.57	1565 (13)	39039	227	0.77	0.57	253 (10)
GC	198582	198288	189428	32807	30700	68	0.71	0.40	80 (7)	2107	2	0.00	0.01	2 (0)
GC2	94053	93926	87922	16162	15575	64	0.83	0.50	71 (5)	587	1	0.00	NA	1 (0)
7CMcore	135254	135086	133629	202	136	16	0.55	0.50	19 (3)	66	1	0.00	NA	1 (0)
7Gt2	150640	150409	138429	14250	7334	33	0.64	0.43	36 (4)	6916	18	0.64	0.48	19 (1)
NEGATIVE CONTROL A	106471	105571	96569	94348	2876	19	0.69	0.49	26 (7)	91472	351	0.97	0.69	461 (36)
NEGATIVE CONTROL B	149421	148866	140175	135739	2782	16	0.83	0.72	17 (2)	132957	484	0.97	0.72	555 (20)
Eukaryotic sequences														
8Ass	320243	319549	312333	307451		306	0.68	0.25	308 (2)					
Ass	148963	148396	142049	140678		122	0.65	0.31	136 (7)					
PS	83526	83207	82325	82316		50	0.06	0.04	55 (4)					
PS3	87971	87459	86745	54		6	0.36	0.46	6 (0)					
Gt	15063	14998	14883	1795		4	0.25	0.34	4 (0)					
8Gt	57995	57773	56359	56269		125	0.56	0.23	125 (0)					

Extended Data Table 4 | Mineral phases observed by SEM-EDX in precipitates of typical abiotic morphology and biomorphs'. Biomorphs correspond to rounded-shaped crystalline morphs resembling cell structures (cocci, rods) and compatible with cellular sizes. Observed dominant phases are highlighted in bold

Site	Samples	Mineral phases	
		Typical 'crystals'	Abiotic 'Biomorphs'
Cave water	Gt2016, 7Gt, 8Gt_1	Si, Ca sulfate, Fe-K sulfate, Al-Mg Fe oxides, Fe and Ca oxides	Fe-Al silicates
Lake Assale (Karum)	8Ass_2, 8Ass_3, 8Ass_4, 8Ass_6, 8Ass_7, 8Ass_8	NaCl, Na-K-Mg chloride	**Si biomorphs** (and encrustment)
Dallol dome (ponds)	Dal4.0, 7DA7_07, DAL4D, 7DA9-P1, 7CA9_P1_3, 7DA7_04, 7DA7_05, 7DA7_06, 7DA9_P1_2, 7DA9_P1_5, 7DA9_P3_10, 7DA9_P3_12	NaCl, Na-K-Mg chloride, Fe-K oxides, Ti oxides	Sulfur biomorphs, **Si biomorphs**, S-rich Na-K silicates, locally S-rich Si biomorphs, **Fe phosphates**, Fe-K phosphate, Si biomorphs – enriched in Fe, Mg, K and locally S
Yellow lake	YL1-03_4, 7YL_4, YL1-03_5, 7YL_6	Fe chloride, Mg chloride	Si, $CaCl_2$, Ca phosphate
Black lake area (ponds)	BLPS_05_5	Mg-Fe-K chloride	Mg chloride